Investigations on Reactive Power and Dead Time Compensation for a Double Active Bridge with a Planar Transformer

by

Javier Gómez-Aleixandre Tiemblo

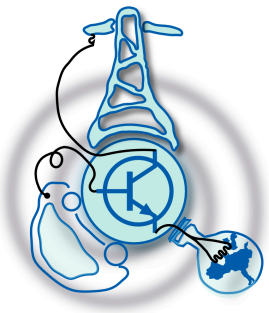

Submitted to the Department of Electrical Engineering, Electronics, Computers and Systems
in partial fulfillment of the requirements for the degree of

Master of Science in Electrical Energy Conversion and Power Systems

at the

UNIVERSIDAD DE OVIEDO

July 2014

Author .....

Certified by .....

Pablo García Fernández
Associate Professor
Thesis Supervisor

Investigations on Reactive Power and Dead Time Compensation for a Double Active Bridge with a Planar Transformer

by

Javier Gómez-Aleixandre Tiemblo

Submitted to the Department of Electrical Engineering, Electronics, Computers and Systems
on July 30, 2014, in partial fulfillment of the
requirements for the degree of
Master of Science in Electrical Energy Conversion and Power Systems

Abstract

In the future, the power system will be a set of intelligent grids (smart grids) with the generation close to the demand (micro grids). The ultimate goal will be to accomplish most of the energy demand with clean and renewable sources. The problem of this energy sources is that they are volatile, and thus the generation may not match with the demand in some instants. In order to solve this, energy storage systems are required to absorb the extra power when there is more generation than demand, and releasing it in the other case. The objective of this thesis is to study the interconnection between these grids and the energy storage with an isolated power converter. A first overview around the different possible converters is covered in order to justify the selection: a dual active bridge (DAB). The behaviour of the DAB was then explained under different situations. Especial interest is paid in the effect of the dead time in the behaviour of the converter and the excessive reactive power. Finally, a control of the power flow in this converter is tested with a variable load. It is also tested an algorithm to compensate the effect of the dead time.

Thesis Supervisor: Pablo García Fernández
Title: Associate Professor

Acknowledgments

First of all, I would like to thank the research group LEMUR (Laboratory for Enhanced Microgrid Unbalance Research), with all its members, and the Department of Electrical Engineering, Electronics, Computers and Systems, for sharing with me their facilities, equipments and knowledge.

I would also like to express my gratitude to all the teachers from the Master of Science in Electrical Energy Conversion and Power Systems for giving me all the necessary knowledge needed for the development of this Thesis, and much more that I will use in my future career.

I should also thank my supervisor, the Professor Pablo García Fernández, first of all for thinking that I was a good candidate for him. But also for all the help, the explanations, the days in the laboratory, his patience with my errors and a large etcetera.

I couldn't forget my laboratory mates, giving me that practical tricks that are nowhere taught, but everywhere needed. And also my class mates, for two years of hard work together, but with time for fun.

Special thanks I need to give to my parents, pushing me forward in this two years, and specially this last months, helping me to achieve this point in my career. With their example started my passion for engineering, with their thoroughness I achieved good results and with their empathy, the worst days were better.

Finally, I would be eternally grateful to my girlfriend, Alba, the person that better knows me. She has been my escape in the moments of high stress and the stimulus in times of weakness. For being my foundations and my look forward, thank you.

Contents

List of Figures

List of Tables

Chapter 1

Introduction

1.1 Introduction

Smart grids and micro grids are, with no doubt, the future in energy generation and distribution. One of the desired feature in the electrical network of the future is to supply energy with renewable and non-polluting sources, instead of the fossil fuel based generation systems. This change means that the generation will have a new level of uncertainty, as the power generated by wind and solar depends extremely on stochastic variables. To avoid the collapse of the grid due to the absence of match between generation and demand, one possible solution is the usage of energy storage systems, storing energy when the generation is greater than the demand, and releasing it in the opposite situation.

The usage of the energy storage systems has one big problem: usually, energy storage devices work in DC, while common electric networks operates in AC. Here is where power electronics play their role, interconnecting storage with grid without worrying about voltages and frequencies.

1.2 Objectives

To develop the work of this thesis, a sequential work had to be done. This work represents, in some way, the various objectives that needed to be achieved to reach

the desired goal. This objectives can be summarized in:

State of the art collection: As a first approach, the literature related with the topic will be collected. This collection will cover from a general overview in the topic of power converters, focusing into isolated DC-DC converters and, in particular, focusing on the selected DAB topology. It will be concluded by the analysis of the literature related with the control of the DAB.

Analysis of the converter in open loop: In order to understand the operation of the DAB, the converter model will be simulated and a performance analysis in function of different variables will be carried out. Conclusions will be obtained in order to achieve the thesis objectives.

Impedance measurement of the planar transformer: Measures of the planar transformer will be taken with an impedance analyser. The relevant impedance parameters will be obtained in order to build a model of the transformer.

Control strategy design and simulation: A control strategy for controlling the power flow in the DAB under different circumstances will be designed. The goodness of the control will be asserted by different simulations.

Physical implementation: A working prototype for a DAB working under low power and low voltage conditions will be built. The operation will be checked in open loop in order to analyse the matching with the proposed model.

1.3 Structure of the document

This master thesis is divided into 5 chapters, with the following structure:

Chapter 1 introduces the main objectives of the thesis and presents the possible opportunities of this topic.

Chapter 2 presents the state of the art of the dual active bridge. Firstly, a brief overview of the DC-DC converters, with a special focus on isolated ones, is covered. Secondly, the solid state transformer concept is explained, and the dual active bridge

is presented. To conclude, the two main problems of the dual active bridge are presented: the reactive power and the dead time.

Chapter 3 covers the modelling of the dual active bridge that is going to be implemented and its control. Initially, the process of how the transformer parameters were obtained is presented. Then, the behaviour of the actual model under different circumstances is described, with special focus on the effect of the dead time on the DAB response. Finally, the control scheme is shown.

Chapter 4 shows the result of various simulations of the power electronics converter, plotting different variables under different operating points, and comparing the control with and without dead time compensation.

Chapter 5 closes this thesis with the extracted conclusions from all the previous work. Also, some possible future works that could be continued from this thesis are presented.

Chapter 2

State of the Art

In this chapter, a general view of the state of the art will be shown. Initially, a general view over different DC-DC converters technology will be covered, paying special attention to isolated DC-DC converters technologies. Then, a further look into solid state transformer technologies will be done, taking specially into consideration the technology of this thesis: the dual active bridge. Finally, the main two problems of the selected technology will be presented.

2.1 DC-DC Converters

Power electronics converters are being more and more widely used. This is because their ability to process and control different types of electrical energy variables and convert them to different ones. This means that the power converters can link a power source to a given load with different characteristics (e.g. a DC load connected to the AC grid). This fact make the power electronics an ideal component for the management of new technologies, such as FACTS, HVDC, microgrids... as they can interconnect different devices with different electrical variables, like solar and wind generation, batteries or a microgrid.

A first possible classification of the power converters can be done depending on the form (frequency) of the the input and output signals [10]. They can be:

- AC to DC

- DC to AC
- DC to DC
- AC to AC

In this thesis, only the DC to DC converters will be considered, as they are the ones that match the first requirement for the converter, interconnection between two DC buses.

Another requirement that need to be matched is the isolation between the two DC buses. This could be due to different reasons, but one of the most important is the security, both for the devices and the users. Because of the need of isolation, many of the well known non-isolated DC-DC power converters; like buck, boost, Cuk or full-bridge [10]; are not taken into consideration.

2.1.1 Isolated Bidirectional DC-DC Converters

The topology of a generic isolated bidirectional DC-DC converter is shown in Fig. 2-1. Here, two DC-AC converters are linked with a high frequency transformer that provides the needed galvanic isolation. In this way, the final converter is actually a DC-AC-DC converter, but it can be considered as a DC-DC converter as the AC part has no effect outside the converter [7, 13, 21].

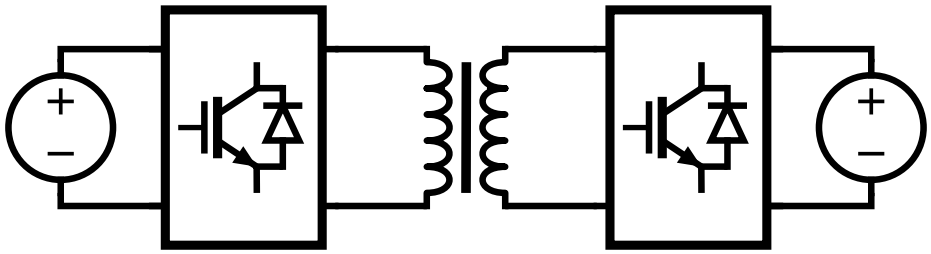

Figure 2-1: Generic isolated bidirectional DC-DC converter topology.

There are different possible classifications of these converters. One which is useful due to its implications in costs and reliability is based on the number of switches [21]:

Dual-switch Dual-flyback, dual-Cuk, Zeta-Sepic

Three-switch Forward-flyback

Four-switch Dual-push-pull, push-pull-forward, push-pull-flyback, dual-half-bridge

Five-switch Full-bridge-forward

Six-switch Half-full-bridge-

Eight-switch Dual-active-bridge

The literature has identified numerous topological alternatives, the three major group of topologies are [13]:

- Flyback converters
- Push-pull converters
- Bridge converters (Half-bridge, Full-bridge, etc.)

The literature [7, 13] conclude that the choice of the converter topology should be based on the required ratings.

Table 2.1 summarises the converter structures and the appropriate limits of each topology that has been analysed in the literature. At low voltage and power levels, flyback converters are popular, but as ratings increase beyond $100V$ and $1kW$, current fed push-pull converters and half-bridges become more appropriate. As voltage and power levels rise still further ($400V$, $2kW$ and above), full-bridge converters become the topology of choice.

Table 2.1: Converter topology comparison.

	Flyback	**Push-pull**	**Half Bridge**	**Full Bridge**
Voltage Rating	Low ($< 100V$)	Low ($100 - 400V$)	Low ($< 100V$)	High ($> 400V$)
Power Rating	Low ($\approx 500W$)	Medium ($\approx 2kW$)	Medium ($\approx 2kW$)	Medium ($> 2kW$)

After this small review it can be assumed that the best converter topology to be used in technologies related with microgrids and smart grids is the full-bridge. For

this reason, the converter that was studied during the research of this thesis was the previously mentioned.

2.2 Solid State Transformer

The solid state transformer is a power electronic device that replaces the traditional $50/60Hz$ power transformer by a high frequency transformer isolated AC-AC conversion, which is presented in Fig 2-2. The basic operation of the SST is firstly to change the $50/60Hz$ AC voltage to a high frequency one (normally in the range of several kHz to tens of kHz), then this high frequency voltage is stepped up/down by a high frequency transformer with dramatically decreased volume and weight, and finally shaped back into the desired $50/60Hz$ one to connect to the output of the SST (grid, load, etc.). In this direction, the first advantage that SST may offer is the reduced volume and weight compared with traditional transformers [17].

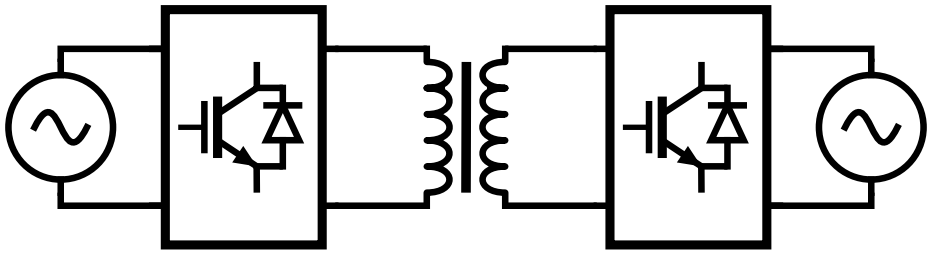

Figure 2-2: Generic solid state transformer converter topology.

But this is not the only possible operation of the SST. The input and output voltages could have variable frequency or even be DC. And also the voltage relation could be from large, step up or down, up to even 1.

The converter that will be studied in this thesis is a particular case of the operations described before. It will be a converter made by two full bridge inverters connected by a high frequency transformer, what is also called dual active bridge.

2.2.1 Dual Active Bridge

As mentioned before, the dual active bridge (DAB) [3] consists on two inverters connected by a high frequency transformer. The scheme of the DAB usually includes an inductor, as seen in Fig. 2-3. This inductor is used to control the power flow between both inverters and will be further explained in the following.

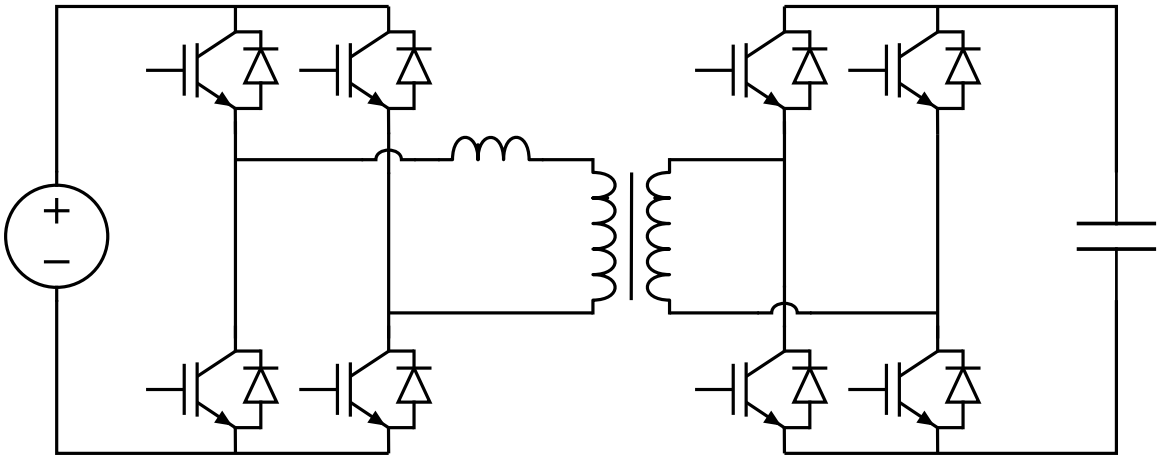

Figure 2-3: Generic dual active bridge converter topology.

This DAB, as previously explained, can be used to control the power flow between the two outputs, in whatever direction. And a very important characteristic is that it can be done in a very short time, with very small transients. With this characteristics, this converter is very well suited for the interconnection of a battery with a microgrid, providing or absorbing power as necessary.

Another important possibility of this converter, is that the transformer can have as many windings as needed, being possible to transfer power to various nodes; but, obviously, increasing its complexity. One possibility, that is being studied [18], is the triple active bridge (TAB), shown in Fig. 2-4. In this case, one possible connection, related with the previous one (battery-DAB-grid), is adding a generator to the scheme. Then, the generator can be used to supply power to the microgrid or to charge the battery, being now much more flexible than the DAB.

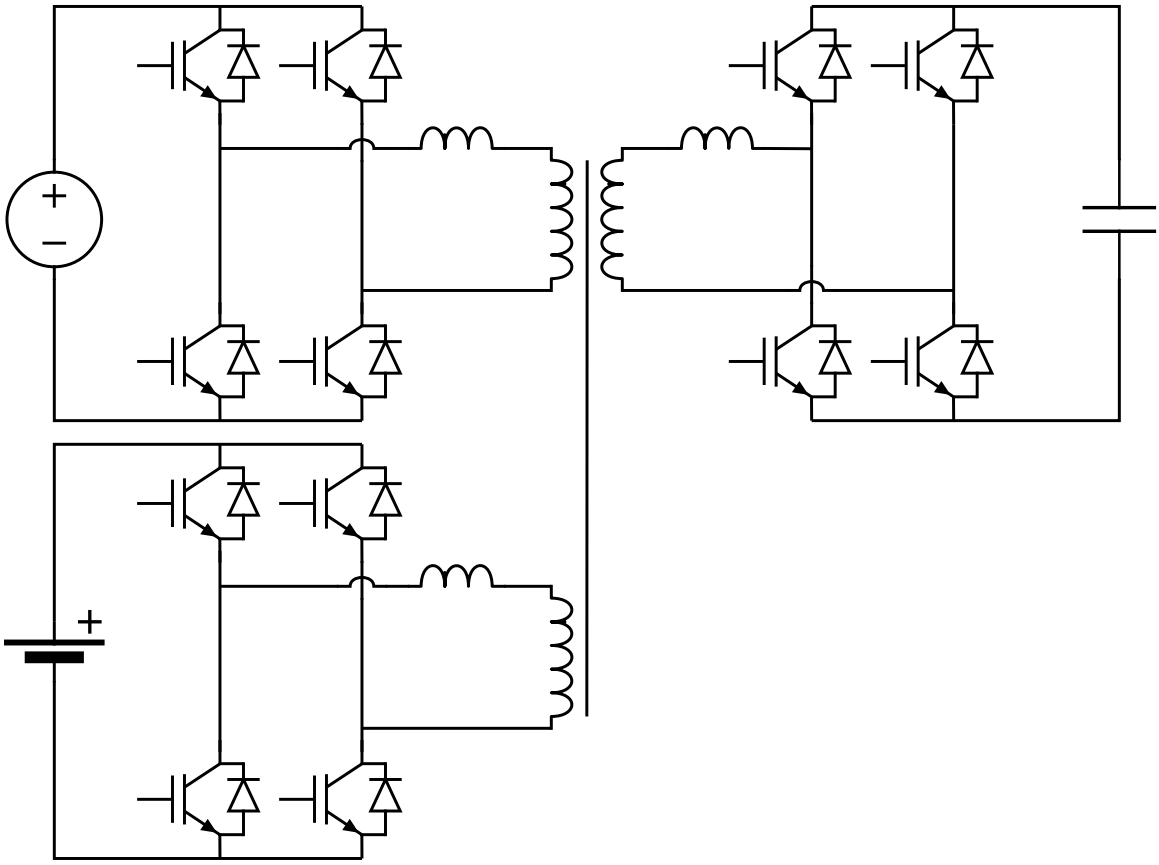

Figure 2-4: Generic triple active bridge converter topology.

DAB Control

The theoretic concept used to control is very well known in electrical engineering: the power trough a transmission line [13]. As said before, the inductor shown in Fig. 2-3 is used for control purposes. This inductor is the equivalent to the transmission line. It is very well known, in the field of power systems, that the power through a transmission line can be described as shown in Eq. 2.1.

$$P = \frac{V_1 V_2 \sin \delta}{X_L} \tag{2.1}$$

Here, V_1 and V_2 represent the voltage amplitudes applied in the nodes of the inductor, δ represents the angle between this two voltages and X_L the impedance of the inductor.

But it is also important to take into consideration the reactive power through the

inductor, described in Eq. 2.2. In transmission lines, this reactive power is useful for different kind of loads or other purposes, but it has no utility in the DAB and will be a problem, as it means an unnecessary current that will produce losses [1, 12]. This problem will be further explained in the following.

$$Q = \frac{V_1 \left(V_1 - V_2 \cos \delta\right)}{X_L} \tag{2.2}$$

Finally, it should be taken into consideration that the most common modulation for the DAB is square wave phase shift, despite others may be used. This means a square wave voltage with 50% duty between $+V_{DC}$ and $-V_{DC}$. For this reason, the active (and reactive) power equation, Eq. 2.1 should be described in terms of harmonics, as shown in Eq. 2.3.

$$P = \sum_{k=1}^{n} \frac{V_{1k} V_{2k} \sin \delta_k}{X_{Lk}} = \sum_{k=1}^{n} \frac{V_{1k} V_{2k} \sin \delta_k}{\omega_k L} \tag{2.3}$$

2.3 Reactive Power and Dead-time Effect in a Dual Active Bridge

This converter, with the mentioned modulation, has two major problems that will be now described:

- Reactive power. The reactive power that will appear when applying the mentioned voltage signals will produce a higher current that will be translated into higher losses, and thus the need of increasing the power ratings of the components.

- Dead time. When using power converters, it is mandatory, in order to avoid undesirable short circuits, to introduce a dead time between complementary signals. This dead time will affect the real δ that is applied to the inductor.

2.3.1 Reactive Power

In the DAB, as it has been said, the modulation is based on applying a square wave to both terminals of the inductor, and by changing the phase between both square waves (assuming that the DC voltages in the DC side of the inverters are constant) the desired active power flow is achieved. However, as Eq. 2.2 shows, there will inevitably be also a reactive power (except when V_1 equals $V_2 \cos\delta$). This reactive power will imply a higher current flowing through the electronic devices, de inductor (if needed) and the transformer. It should be noticed that the reactive current that appears won't have any value, as when the current goes to the DC side of the inverters, the reactive power has no sense.

For this reason, some possible solutions have been proposed in the literature. The most important is described in the following:

Dual phase shift control [1, 11, 12]: By adding a second phase shift between the diagonal switches of each inverter. This means that the voltage applied to each terminals of the inductor won't be a pure square wave anymore, being the voltage equal to 0 in some points. Now, by controlling both phase shifts, a new degree of freedom appears and the reactive power can be annulled while achieving the desired active power.

2.3.2 Dead-time Effect

Finally, another key problem of the DAB is the effect of the dead time between the switches of each arm in the effective δ applied to the inductor. This is due to the fact that, during this dead time, the voltage applied to the inductor by each arm is unknown, as both switches are turned off and the voltage is fixed by the direction of the current that comes from each arm, which should flow through one of the anti-parallel diodes of the switches.

One possible solution, that is going to be implemented in this thesis, is well described in [13]. This solution consists in compensating the effect of the dead time, taking into consideration the known variables to estimate how is going to behave the

system with this dead time, and modifying the applied δ so that the system with dead time behaves as closer as possible to the system with an ideal inverter.

Chapter 3

Model and Control

In this chapter, the physical model of the DAB is obtained and the control strategy explained. First, the impedance model of the planar transformer used to build the DAB is obtained. Then, the behaviour of the actual DAB is presented. Following, the previously mentioned effect of the dead time is shown with the model of the actual DAB and the developed compensation is explained. Finally, the control strategy used to control the power flow in the DAB is shown.

3.1 Transformer Parameters Identification

The first step to develop the model of the DAB is to obtain the exact model of the transformer. The parameters of the physical transformer are presented in Tab. 3.1. It should be pointed that the selected DAB configuration has higher number of turns in the transformer in the side of the secondary bridge, for this reason, what is called the primary side of the transformer should be connected to the side of the secondary bridge and vice versa. As it is intended that the inductance being used for the power flow control is the leakage inductance of the transformer and any transformer parameter can affect the response to the switching applied by the power converters, the model of the transformer should behave as close as possible to the real transformer.

The model used as an initial guide for the estimation was the classic circuit of a transformer, shown in Fig. 3-1. In order to extract the impedances of the transformer,

Table 3.1: Real transformer specifications.

Specification	Value
Manufacturer	Himag
Total output power	10kW
Primary nominal voltage	200V
Switching frequency	20kHz
Turns ratio (Pri-Sec)	22/18

two tests were done in an impedance analyser:

1. No-load test.

2. Short circuit test.

The measurements were done in two different transformers and in their two sides. From now on, as the procedure is the same, only the primary of one transformer will be considered for the impedance estimation.

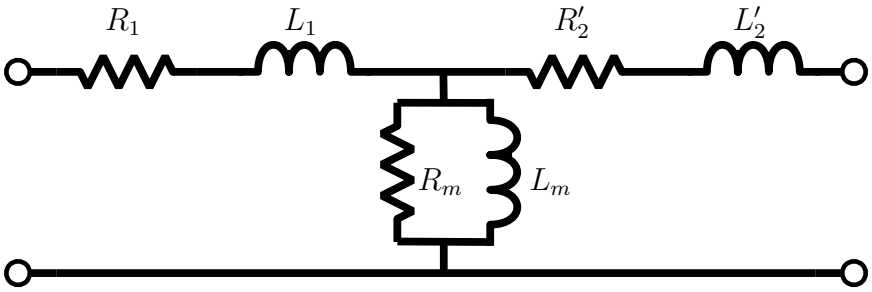

Figure 3-1: Classic impedance model of a transformer.

3.1.1 No-load Test

The first test to be done was the no-load test. In this case, the impedance analyser was connected to what was selected as primary, and the secondary terminals were kept unconnected, as can be seen in Fig. 3-2.

In Fig. 3-3 and 3-4 it can be seen the impedance magnitude and angle that were measured. It is easy to observe the presence of a resonance at a frequency near $100kHz$

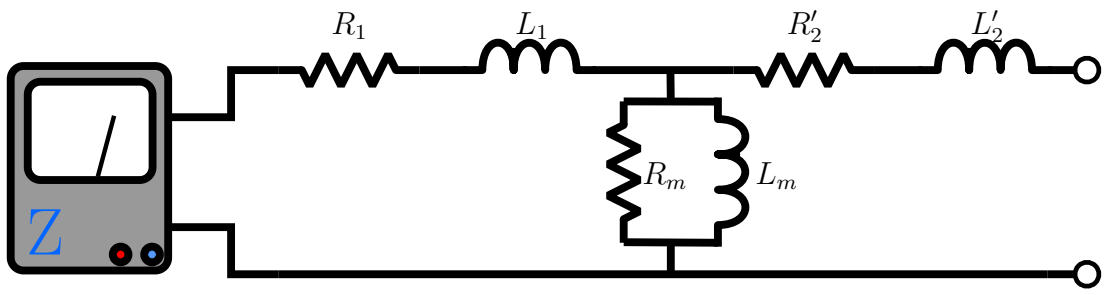

Figure 3-2: Impedance analyser connection for the no-load test.

in the impedance magnitude plot. This implies that, in the magnetizing branch, a parasitic capacitance may be in parallel with the resistance and the inductance (Fig. 3-5).

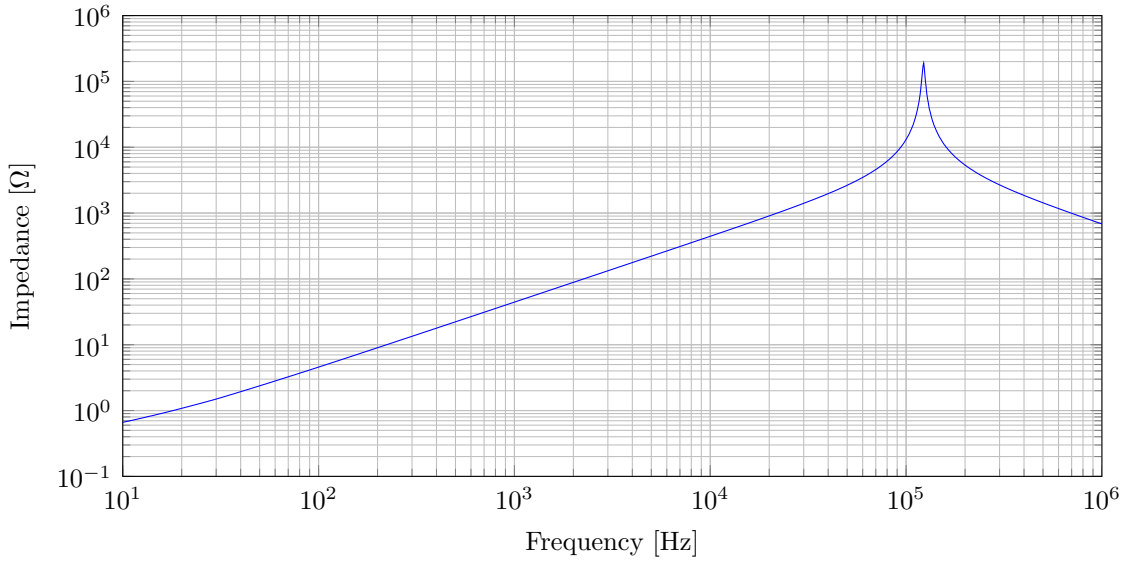

Figure 3-3: Transformer impedance under a no-load test.

In order to make the estimation of the parameters, it was needed to fit the measured impedance to a known equation. Two different models were proposed for the estimation:

1. Assuming that the the leakage contribution to the total impedance value is negligible, the system response is approximated by the impedance of a resistance, an inductance and a capacitance in parallel (Eq. 3.1).

2. Considering the leakage effects on the primary side, (Eq. 3.2).

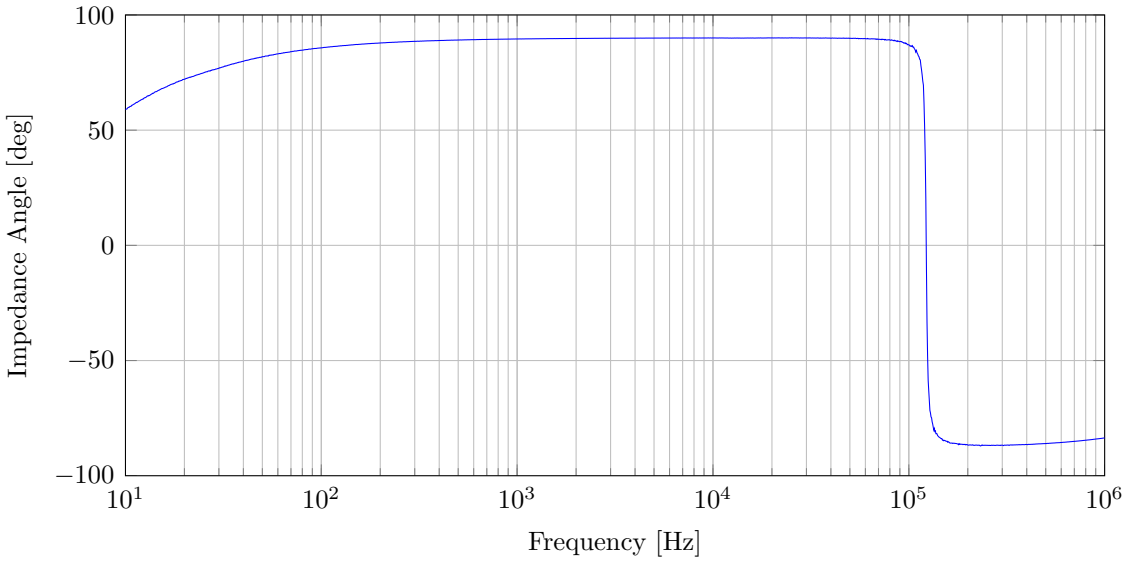

Figure 3-4: Transformer impedance angle under a no-load test.

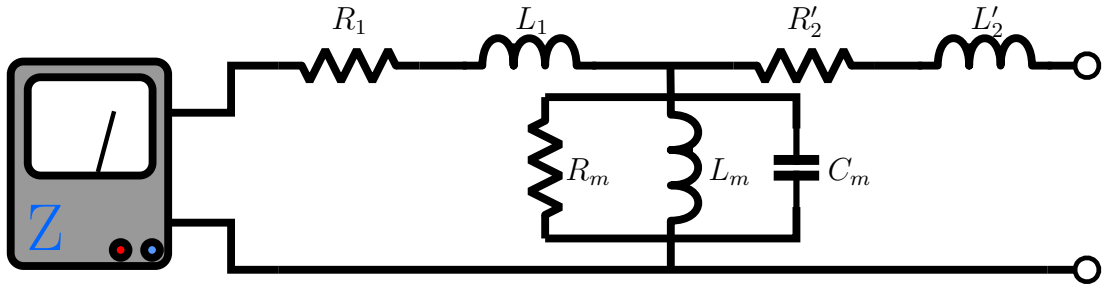

Figure 3-5: Impedance analyser connection for the no-load test with a capacitance in the magnetizing branch.

$$Z(j\omega) = \frac{1}{\frac{1}{R_m} + C_m\omega j + \frac{1}{L_m\omega j}} \tag{3.1}$$

$$Z(j\omega) = R_1 + L_1 j\omega + \frac{1}{\frac{1}{R_m} + C_m\omega j + \frac{1}{L_m\omega j}} \tag{3.2}$$

The estimation was done using both equations, but it was observed that the effect of the leakage part affected mainly the low frequencies in the impedance plot (Fig. 3-6). For this reason, the precision of the leakage inductances was not high enough and only the magnetizing impedances were extracted from this first estimation.

The estimated magnetizing impedances are presented in Tab. 3.2. The goodness of

the fit can be seen in Figs. 3-6 and 3-7. In Fig. 3-6 the precision in the approximation is quite obvious, as the resonant frequency and the resonant peak matches perfectly with the real ones. In Fig. 3-7, the approximation does not look as good as in the previous plot, as at high and low frequencies the real model deviates from the estimated one. However, the approximation around the DAB switching frequency, $20kHz$, is also quite good.

Table 3.2: Estimated parameters of the transformer in the no-load test.

Parameter	**Value**
R_m	$188.2k\Omega$
L_m	$7.044mH$
C_m	$0.2388nF$

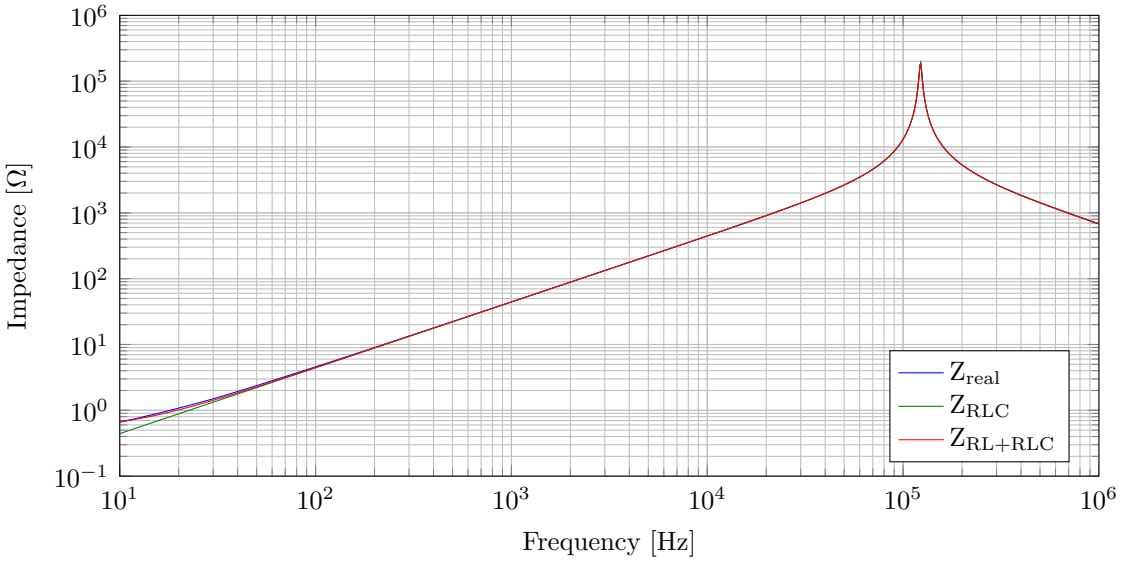

Figure 3-6: Transformer impedance estimation under a no-load test.

3.1.2 Short Circuit Test

The second test was the short circuit test. In this case, the impedance analyser was connected to what was selected as the primary, and the secondary terminals were short circuited, as it can be seen in Fig. 3-8.

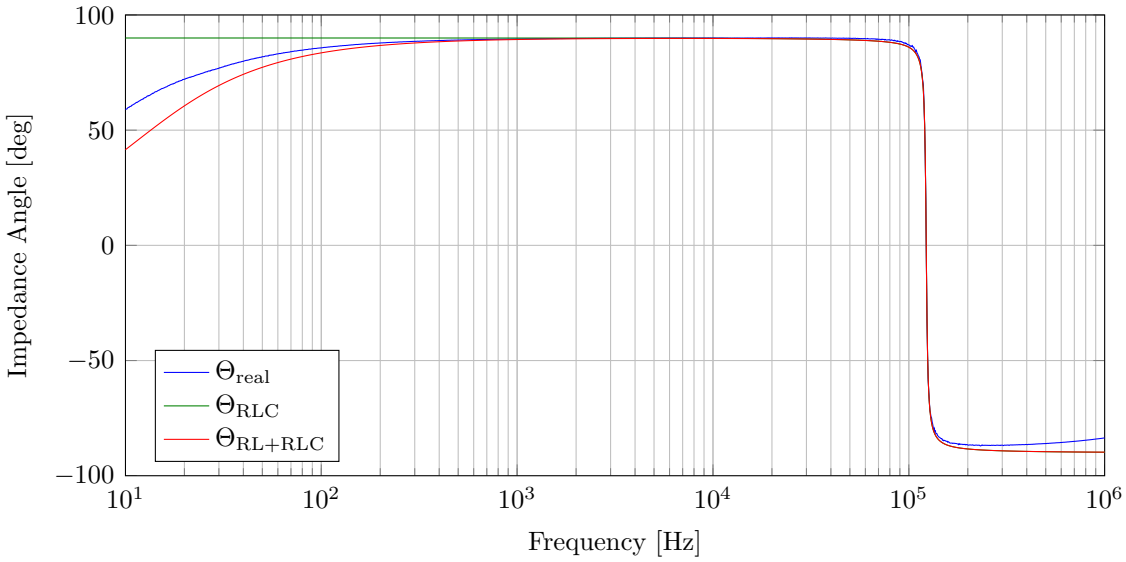

Figure 3-7: Transformer impedance angle estimation under a no-load test.

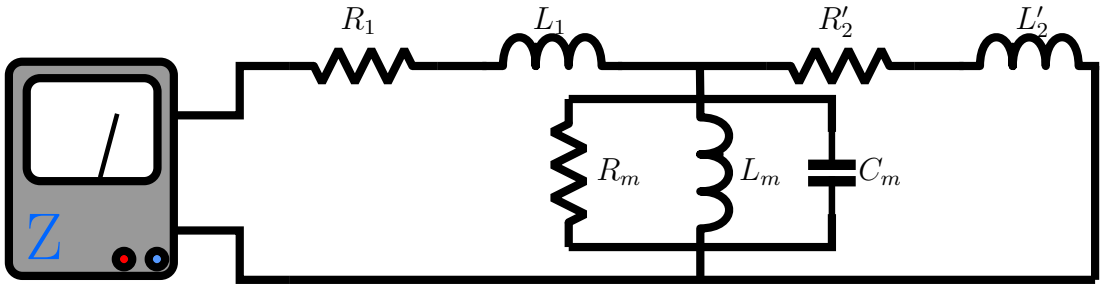

Figure 3-8: Impedance analyser connection for the short circuit test.

In Fig. 3-9 and 3-10 it can be seen the impedance magnitude and angle that were measured.

In order to perform the estimation , it was needed to fit the measured impedance to the equation of a resistance in series with an inductance (Eq. 3.3); neglecting the effect of the magnetizing branch, as the effect of the parallel branch, having a remarkable higher impedance than the leakage path could be considered as an open circuit.

$$Z\left(j\omega\right) = R + Lj\omega \tag{3.3}$$

being $R = R_1 + R'_2$ and $L = L_1 + L'_2$.

The estimated leakage impedances are presented in Tab. 3.3. As it is impossible

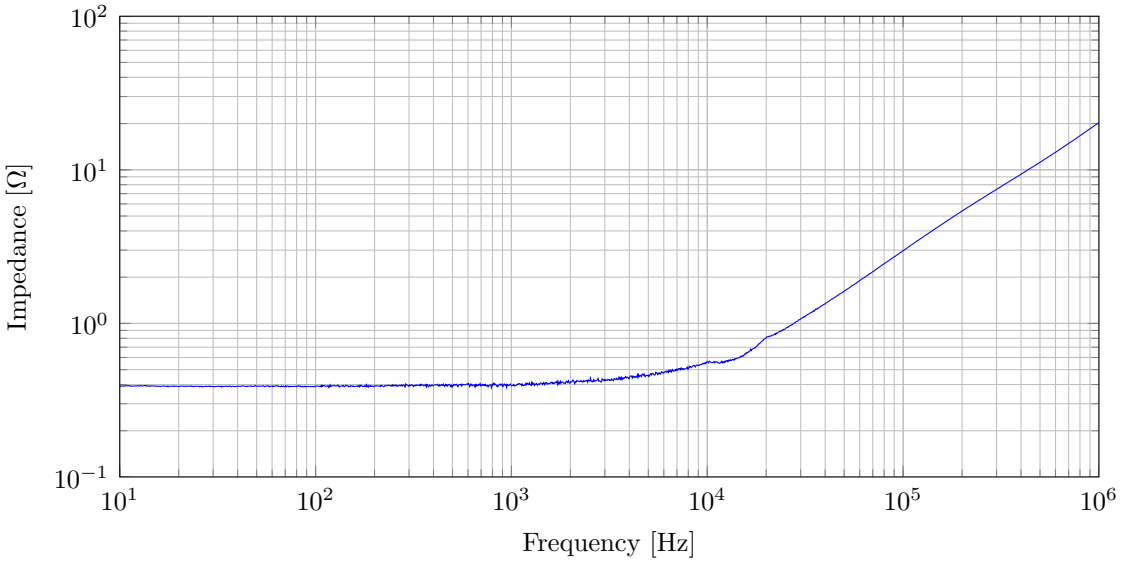

Figure 3-9: Transformer impedance under a short circuit test.

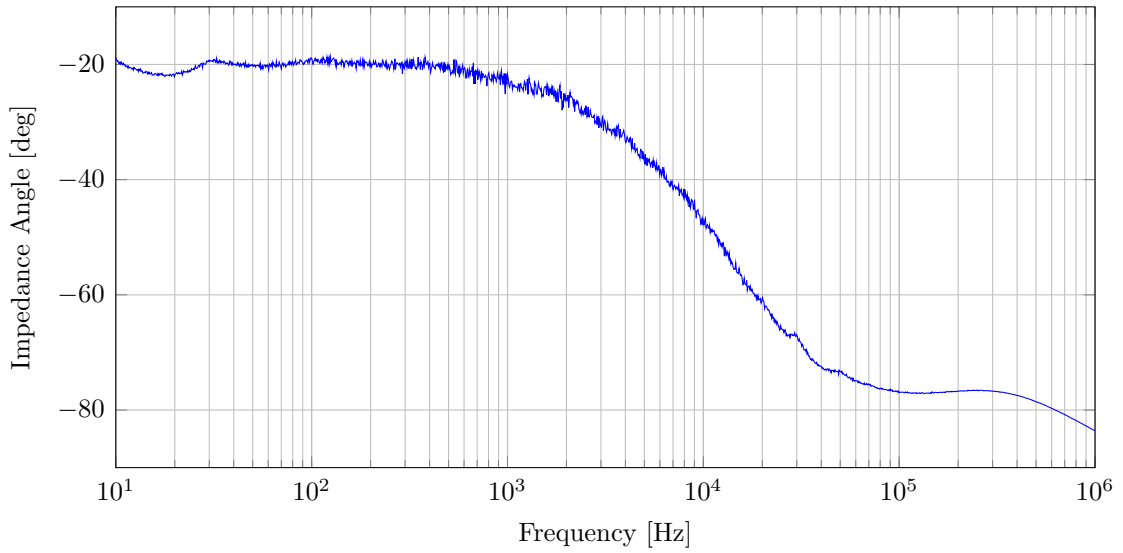

Figure 3-10: Transformer impedance angle under a short circuit test.

to distinguish between R_1 and R'_2, and L_1 and L'_2 in the estimation, as it would lead to an infinite number of solutions, it is decided to make $R_1 = R'_2$ and $L_1 = L'_2$ as they are often quite similar values. In 3-11 it can be seen how the estimation follows the real impedance quite well up to frequencies above the switching frequency. However, the estimation in the angle seen in Fig. 3-12 is far from being good. This is due to numerous non-linearities that appear in the angle that makes a challenging task to

fit the real impedance (both magnitude and angle) to a known model. It should be pointed that, despite the impedance angle is improved by including the magnetizing branch, as shown in Fig. 3-14, the model is not sufficiently accurate (the impedance magnitude is still valid with the magnetizing branch, as shown in Fig. 3-13). But, anyway, this model was accepted as the lack of non-linearities knowledge makes really hard to achieve a better estimation.

Table 3.3: Estimated parameters of the transformer in the short circuit test.

Parameter	**Value**
R_1	0.2Ω
L_1	$2.5\mu H$
R_2'	0.2Ω
L_2'	$2.5\mu H$

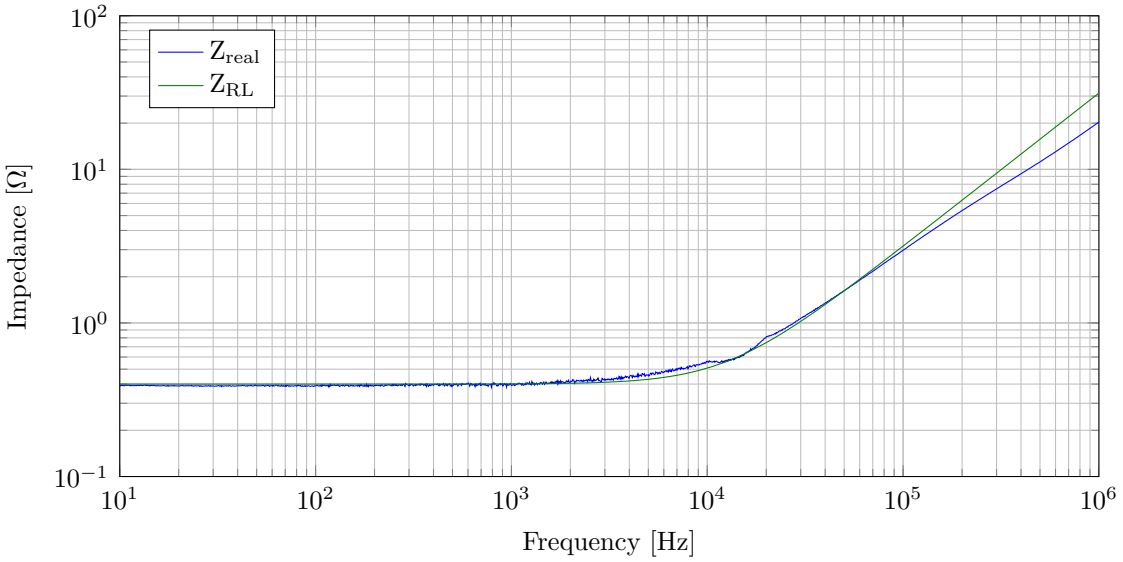

Figure 3-11: Transformer impedance estimation under a short circuit test.

3.1.3 Final Transformer Estimation

Finally, and as a summary, all the transformer parameters and its model are shown in Tab. 3.4 and Fig. 3-15 respectively.

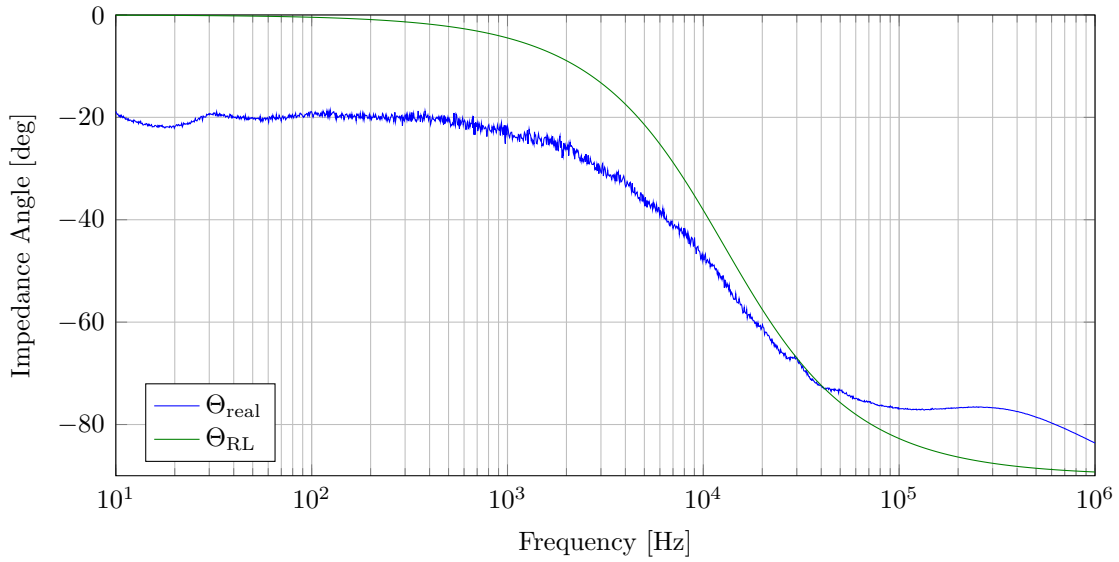

Figure 3-12: Transformer impedance angle estimation under a short circuit test.

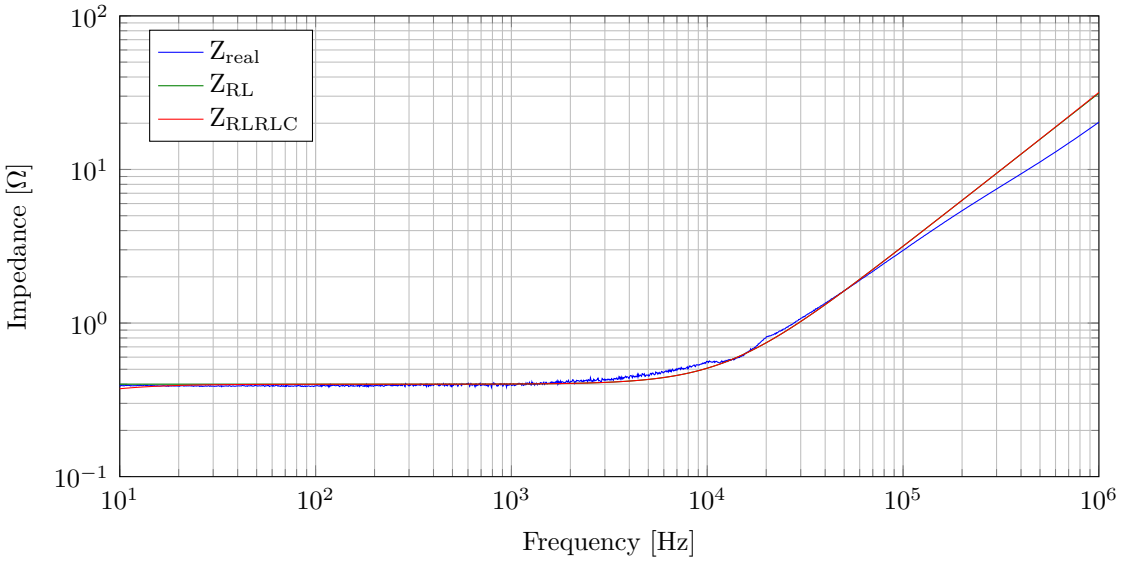

Figure 3-13: Transformer impedance estimation under a short circuit test including the magnetizing branch.

3.2 DAB Modulation

Before starting with the model of the DAB, a fast overview through its modulation should be taken. As it has been said before, the modulation of this power converter is straightforward: two 50% duty cycle pure square waves between $+V_{DC}$ and $-V_{DC}$ are applied to the terminals of the inductor (with the transformer connected to one

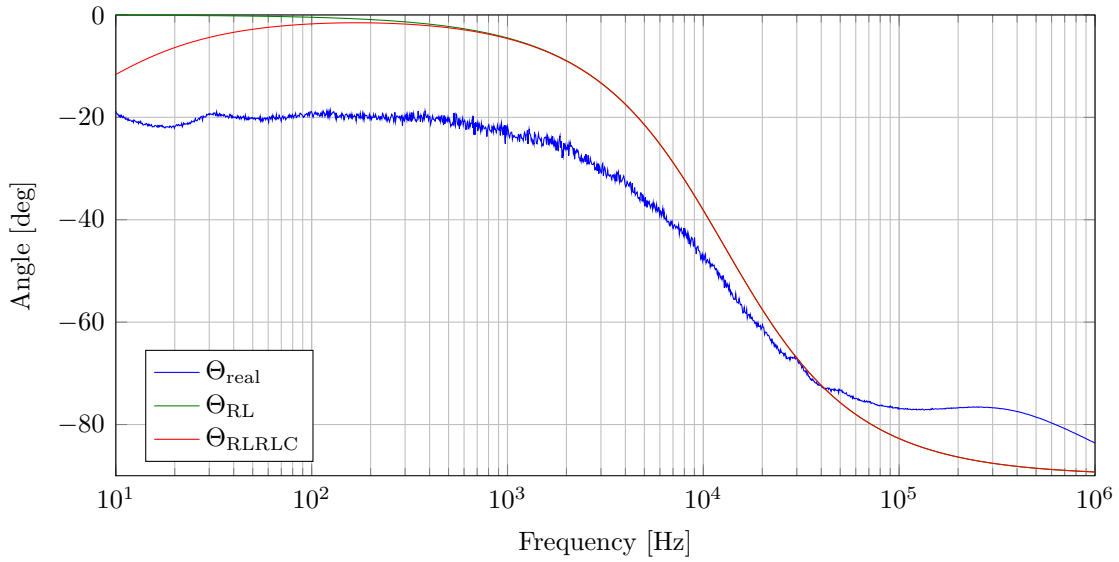

Figure 3-14: Transformer impedance angle estimation under a short circuit test including the magnetizing branch.

Table 3.4: Estimated parameters of the transformer.

Parameter	**Value**
R_1	0.2Ω
L_1	$2.5\mu H$
R'_2	0.2Ω
L'_2	$2.5\mu H$
R_m	$188.2k\Omega$
L_m	$7.044mH$
C_m	$0.2388nF$

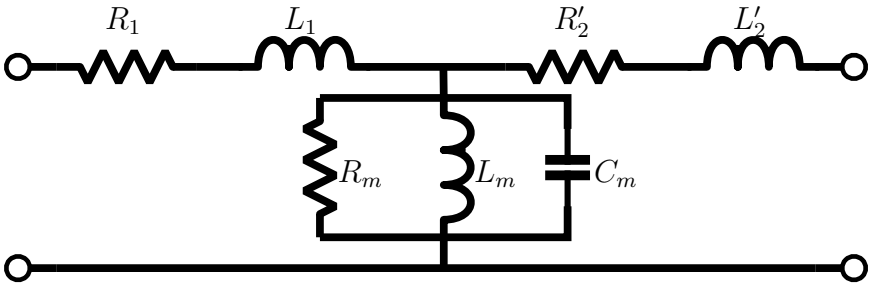

Figure 3-15: Final impedance model of the transformer.

terminal) and this square waves have a phase lags between them. This phase lag will be the responsible of the power flow in the DAB.

In the following, some plots will show the modulated voltages applied to the inductor and the resulting current in the primary and secondary of the transformer.

In Fig. 3-16, the applied voltages have the same phase, as can be easily seen. As the transformer has not a unitary turns ratio, there is a square wave voltage of the same shape as the modulated voltages, but different magnitude, applied to the inductor. For this reason, a current appears in the inductor. As the real inductor has a resistive part, the shape of the current is a sequence of exponentials. The lower the resistive part, the closest the shape of the current to a triangular wave.

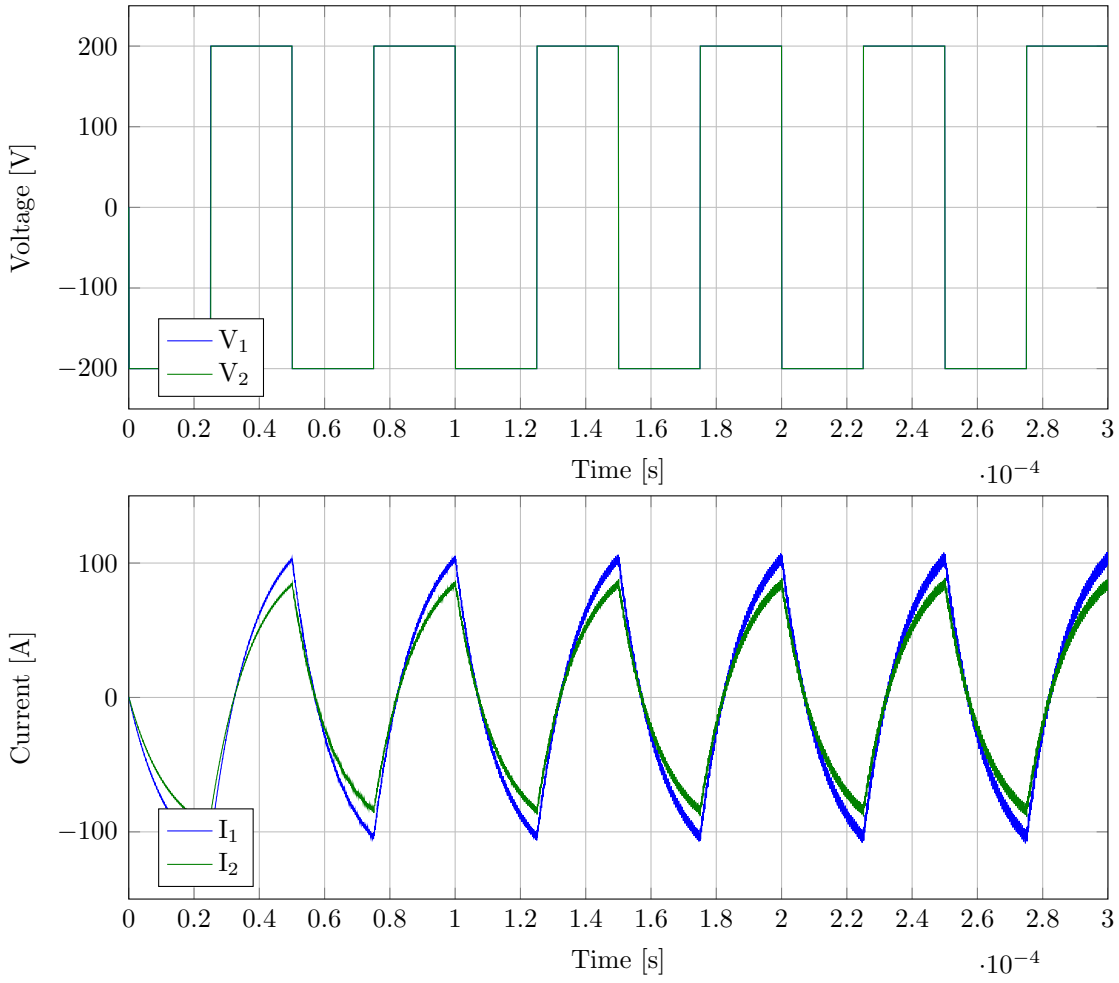

Figure 3-16: Voltages and currents in the primary and secondary of the transformer with 0° commanded phase lag and without dead time.

In Fig. 3-17, now the voltages have a phase difference of 20° (the voltage of the primary bridge leads the voltage of the secondary). Here, the current increases, or

decreases, quite fast when the instantaneous voltages of the bridges have the opposite sign. Then, the current decreases in magnitude as an exponential and tends to the same value than the previous current. As before, if the resistive component of the inductor decreases, the current when the instantaneous voltages of the bridges are equal will increase as a straight line.

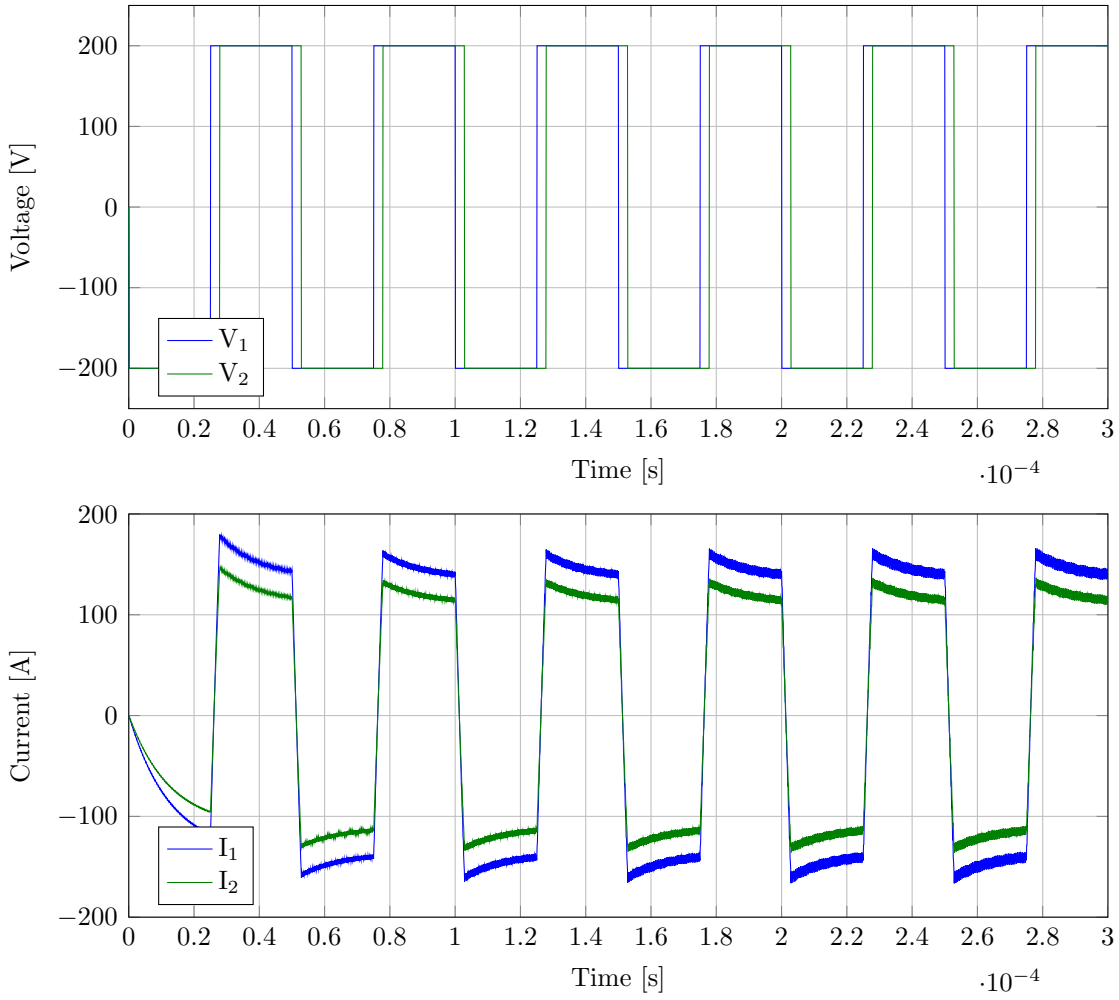

Figure 3-17: Voltages and currents in the primary and secondary of the transformer with 20° commanded phase lag and without dead time.

In Fig. 3-18, now the voltages have a phase difference of −20° (the voltage of the primary bridge lags the voltage of the secondary). Now, the current increases in magnitude slowly first, when the instantaneous voltages applied by the bridges are equal, and then faster when the sign of the voltages becomes the opposite.

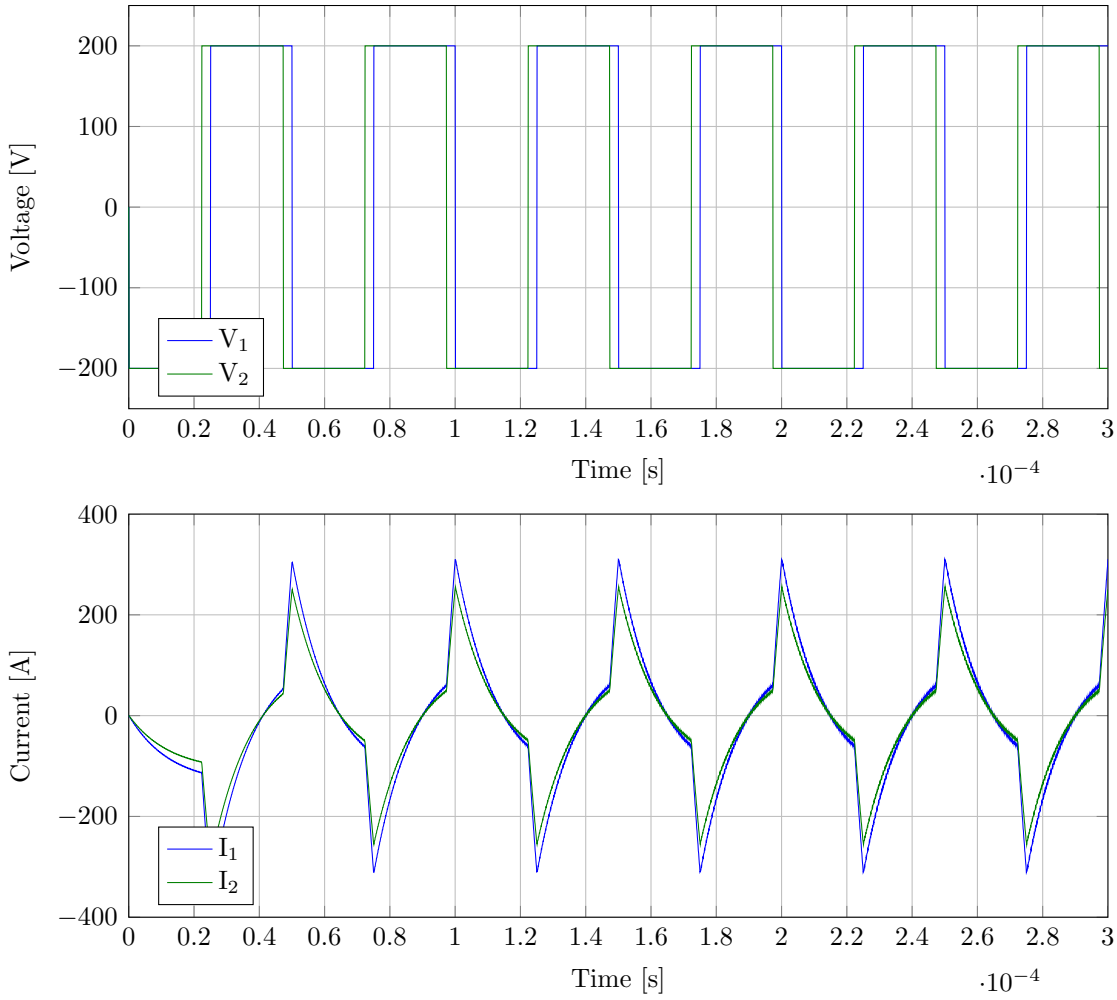

Figure 3-18: Voltages and currents in the primary and secondary of the transformer with $-20°$ commanded phase lag and without dead time.

3.2.1 Effect of the Dead Time in the Modulation

Now, the same situations were plotted, but the power converter have a dead time in their gate signals of $2\mu s$. With this new graphs, the effect of the dead time in the current, that in the end will mean an effect in the transfer of power, will be shown. It should be pointed that the $2\mu s$ at the selected frequency ($20kHz$) is equivalent to an angle of $14.4°$, almost a 75% of the selected phases commanded in 3-17 and 3-18.

In Fig. 3-17, the applied voltages have the same phase again. But the dead time makes the voltages to oscillate during its duration. This is because, during the dead time, the voltage applied by the bridge depends on the current direction, as it is fixed

by the diodes. It can be easily seen in the current: when the current is negative (positive from the point of view of the secondary bridge, as the current is measured exiting the primary bridge, but entering the secondary), the voltage applied by the primary bridge is $+V_{DC}$ and by the secondary $-V_{DC}$. Then, the current oscillates around 0 until the dead time disappears. The same, but with opposite sign happens when the current is positive.

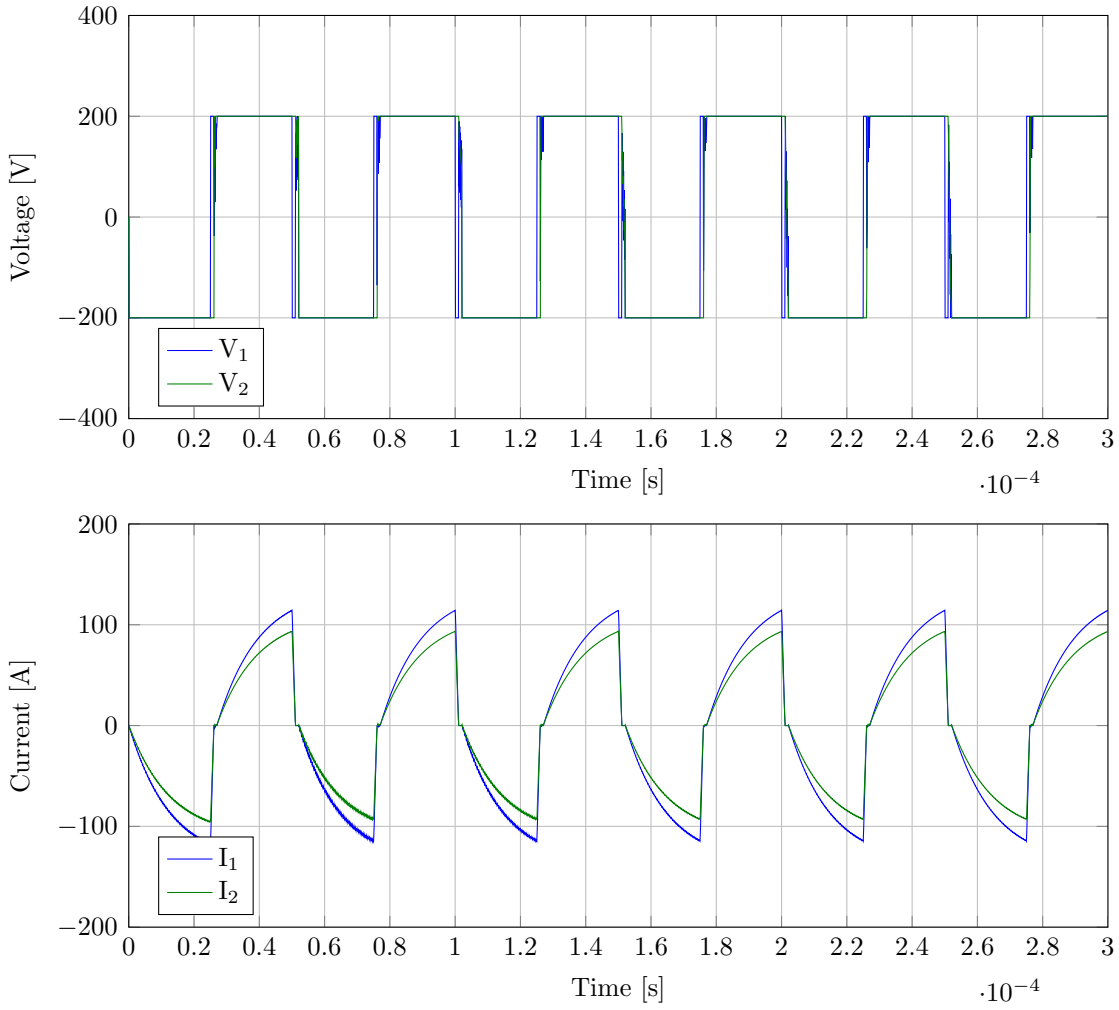

Figure 3-19: Voltages and currents in the primary and secondary of the transformer with 0° commanded phase lag and with $2\mu s$ dead time.

In Fig. 3-20, with a 20° phase lag, the situation is the same than the explained before. When the dead time starts, the current reaches fast $0A$ and then keeps oscillating around this value until the dead time finishes. In this case, the shape of

the current is not highly distorted. However, the magnitude is around a 30% less than the value with no dead time, and so would be the power.

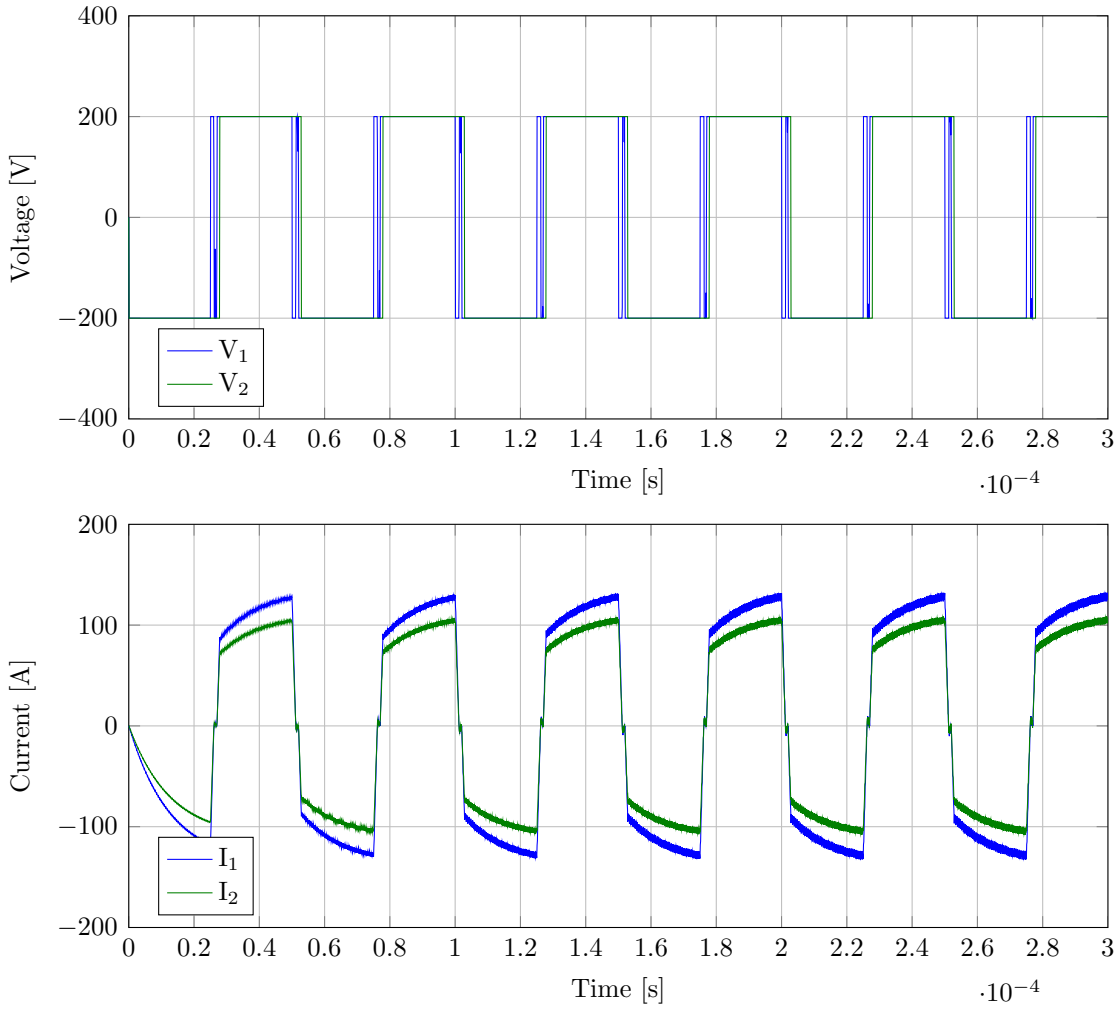

Figure 3-20: Voltages and currents in the primary and secondary of the transformer with 20° commanded phase lag and with $2\mu s$ dead time.

In Fig. 3-21, with a $-20°$ phase lag, happens more or less the same than with 20°: the shape of the current is not highly distorted, but the magnitude is considerably reduced, around a half of the current without dead time.

3.2.2 Current Harmonics Due to the Modulation

As it has been seen in Figs. 3-16 - 3-21, the content of harmonics of the current is quite high. But, however, it differs between different angles, having completely

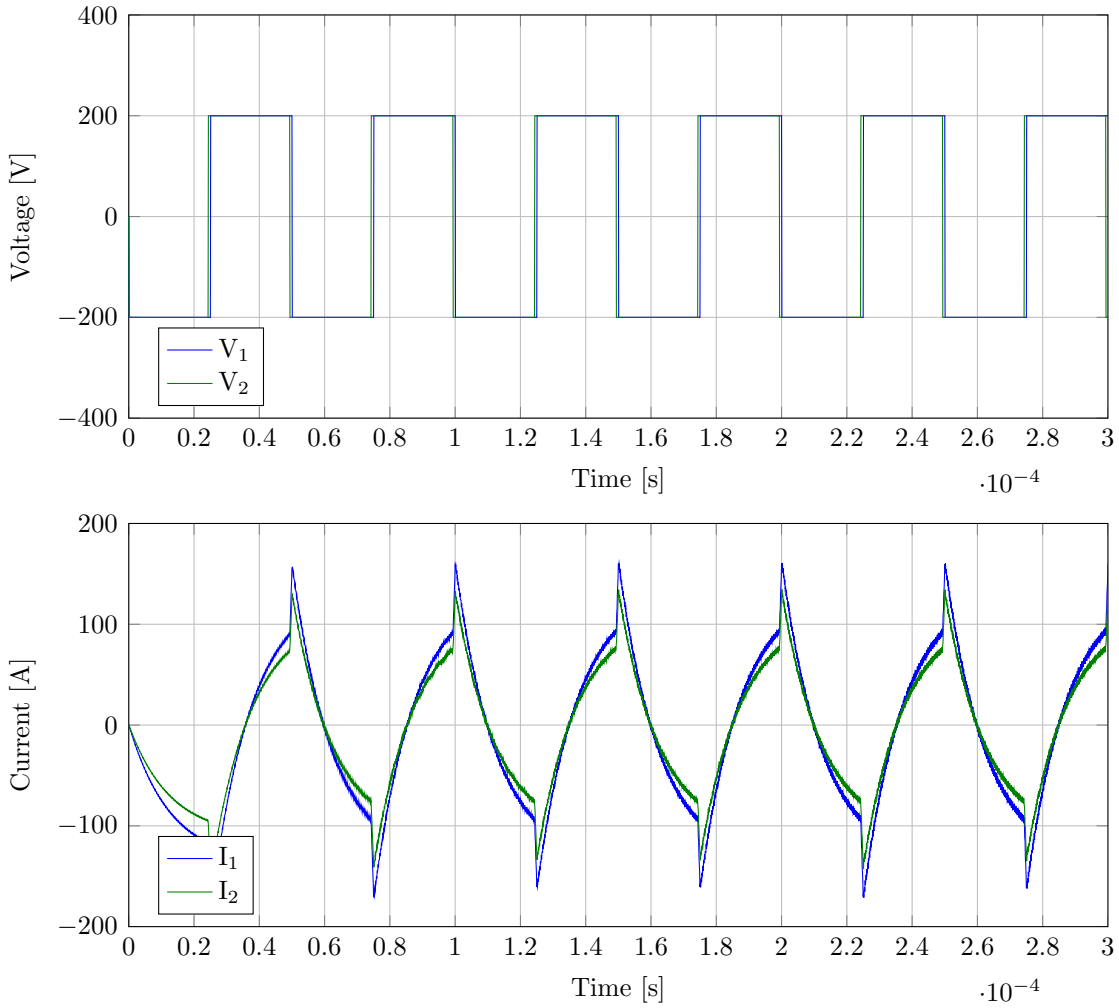

Figure 3-21: Voltages and currents in the primary and secondary of the transformer with $-20°$ commanded phase lag and with $2\mu s$ dead time.

different shapes for the three plotted phases.

For this reason, a fast look of the harmonic content of the current is shown in Fig. 3-22. As can be seen, the content of harmonics is very variable. The THD with no dead time has a symmetric shape, centred in 0°. In this point there is a relative minimum, caused by the fact that the voltages are in phase, and thus the current shape is close to a triangular wave, which has a low THD. Two maximums appear in $\pm 18.75°$, due to the poor quality of the wave (currents close to this angle can be seen in Figs. 3-17 and 3-18). Another maximum, relative in this case, appears in $\pm 180°$; however, the THD value is the same as in the relative minimum in 0°, as in this point

the voltages are in anti-phase and the shape of the current (not the magnitude) is the same that in that minimum. Finally, two absolute minimums appear near $\pm 120°$, due to the fact that in this point the voltage across the inductor is like a three-level signal with 50% duty and the shape of the current generated by this signal is close to a sinusoidal (Fig. 3-23).

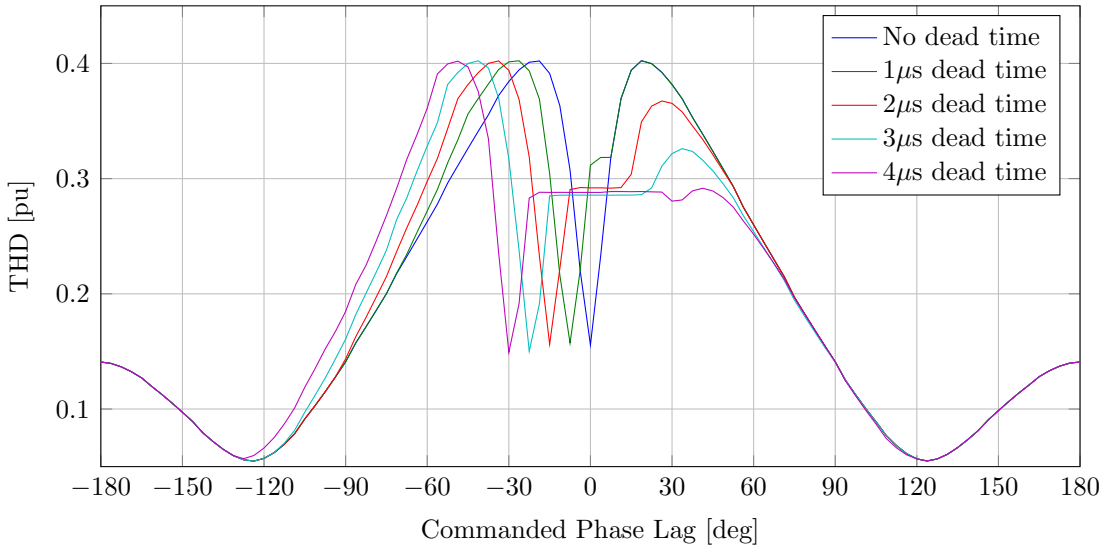

Figure 3-22: Total harmonic distortion at different commanded phase lags with different dead times.

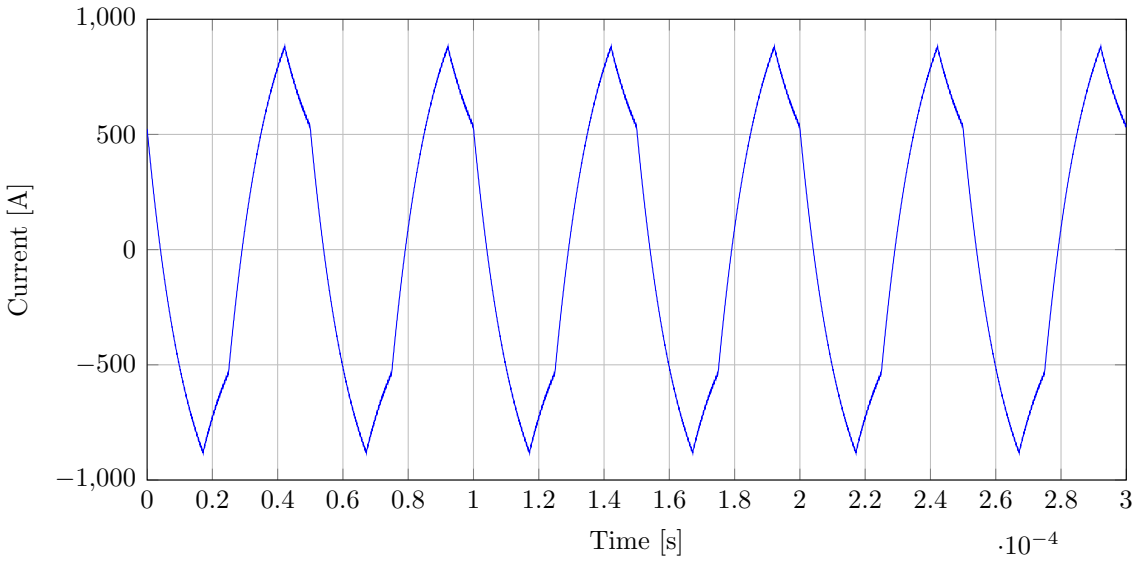

Figure 3-23: Currents in the inductor with 120° commanded phase lag and no dead time.

The effect of the dead time in the THD is clearly not symmetrical. This is due to the fact that the dead time is equivalent to an added phase, but this phase has always the same direction. The effect is considerable at low angles, and decreases as the phase increases. First of all, the relative minimum is shifted to the left as the dead time increases, because it "misleads" the converter like if the applied voltages were in phase at lower angles. The left maximum is also shifted because of the same reason. However, the right maximum is minimized, in this case the phase seen by the inductor is lower (it can be checked in Figs. 3-17 and 3-20). At high angles, as expected, the effect of the dead time is negligible.

In Figs. 3-24, 3-25 3-26 and 3-27, the harmonic content of the current in the left absolute maximum and the right absolute minimum without dead time and with $4\mu s$ dead time are respectively plotted in order to illustrate the previously mentioned information. It is clear that, both maximum and minimum are equal independently of the presence of dead time.

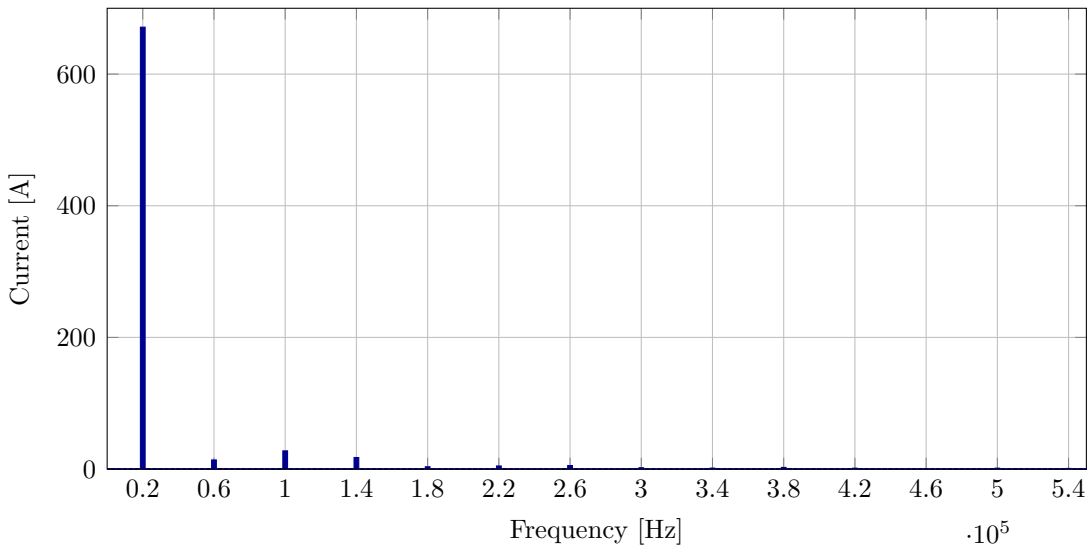

Figure 3-24: Harmonic components of the current with 123.75° commanded phase lag and no dead time.

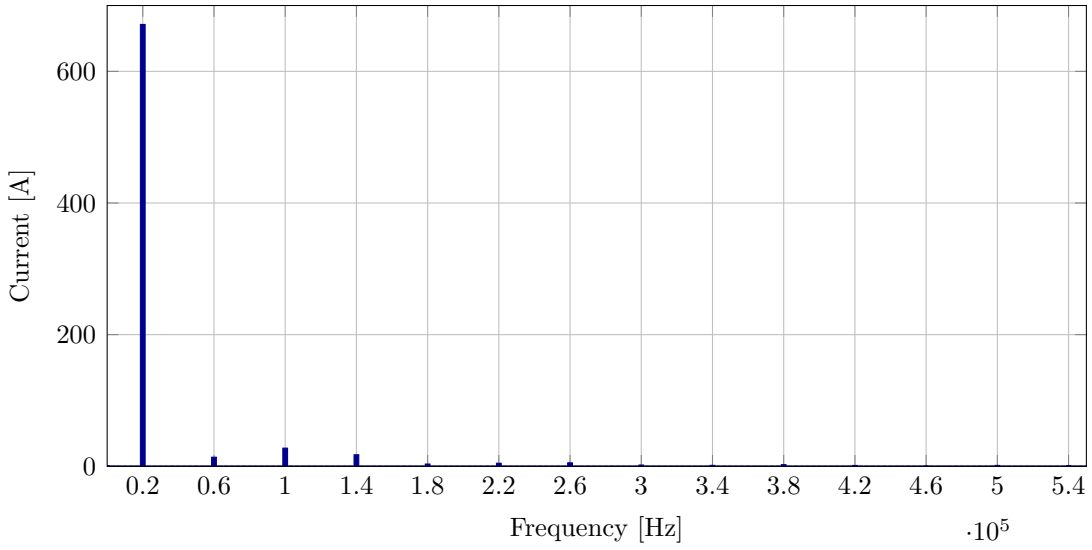

Figure 3-25: Harmonic components of the current with 123.75° commanded phase lag and with $4\mu s$ dead time.

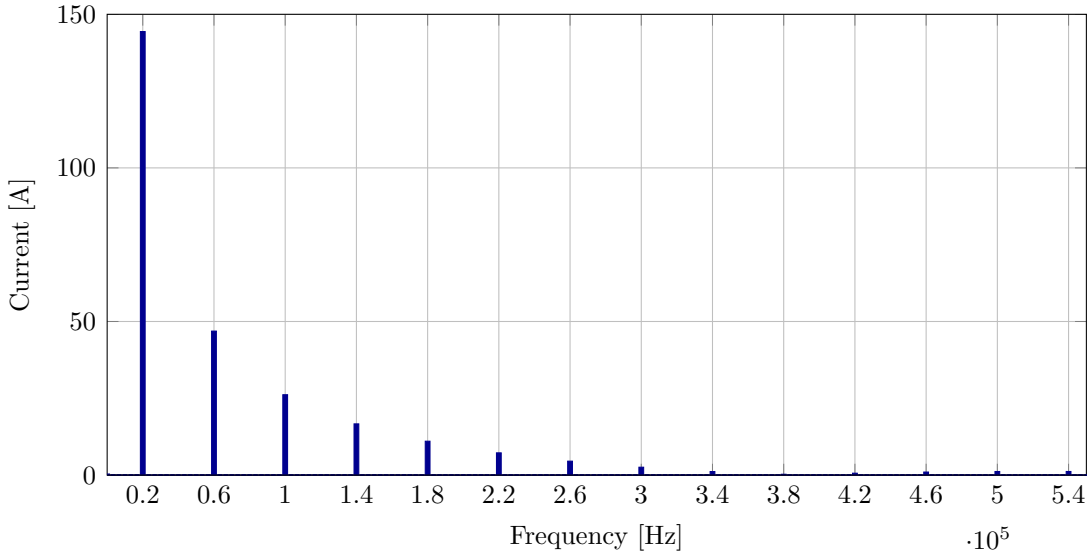

Figure 3-26: Harmonic components of the current with $-18.75°$ commanded phase lag and no dead time.

3.3 Actual DAB Model

Once the model of the transformer was obtained, now its response integrated into the DAB power topology will be shown. In Figs. 3-28 and 3-29 it can be seen, respectively, the active and reactive power flowing into the secondary bridge of the DAB. This figures were obtained by applying the classical square-wave phase-shift

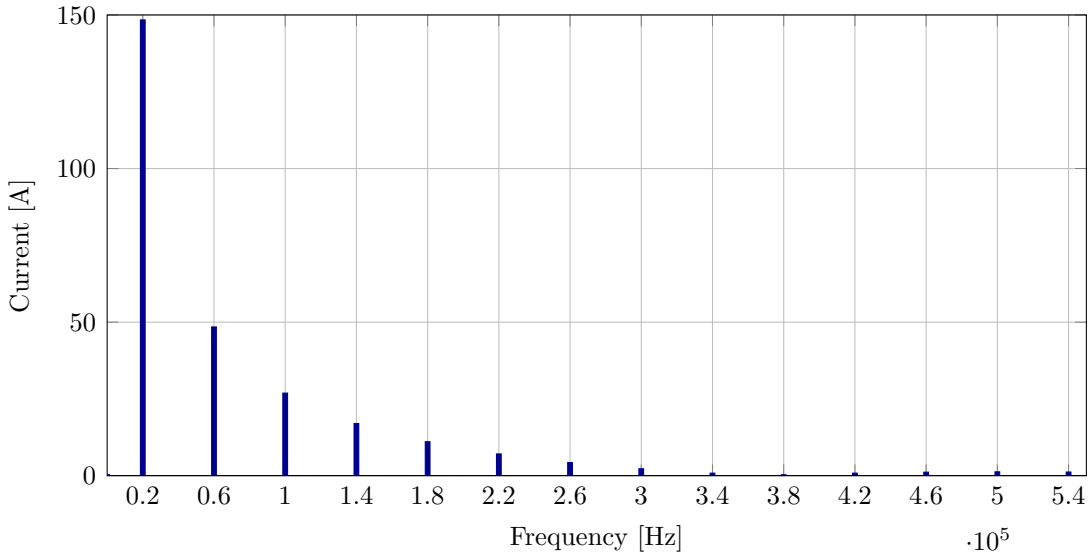

Figure 3-27: Harmonic components of the current with $-48.75°$ commanded phase lag and with $4\mu s$ dead time.

(SWPS) modulation, where two square waves with 50% duty were applied to the primary and secondary bridges with a selected phase between them. However, these values do not match with the ones presented in the previous chapter.

Especial attention should be paid to the huge amount of reactive power that is flowing through the transformer, having maximum reactive currents even bigger than the maximum active currents. All this reactive power does not contribute at all to the operation of the DAB, but just meaning greater losses and greater power ratings in all the power components. In Figs. 3-30 and 3-31 it can be seen the amount of the current that is flowing through the DAB that transport no power to the output of the converter. This amount is quite huge and completely unacceptable. For this reason, in further development of the control designed in this thesis, extra considerations will be required to mitigate the reactive power.

It is easy to see that the shape of the active power is not the shape of a pure sinusoidal. This effect is due to due presence of the leakage resistance, being in the same range of the leakage reactance.

In the following, applying basic electrical theory and trigonometry, the real power flow equation is going to be extracted.

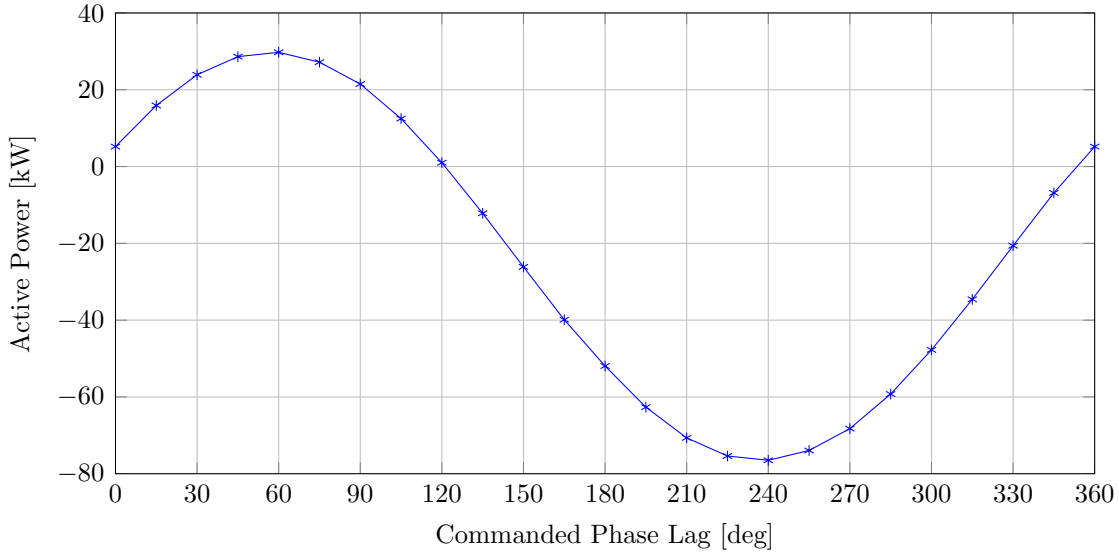

Figure 3-28: Active power entering the secondary bridge under different commanded phase lags.

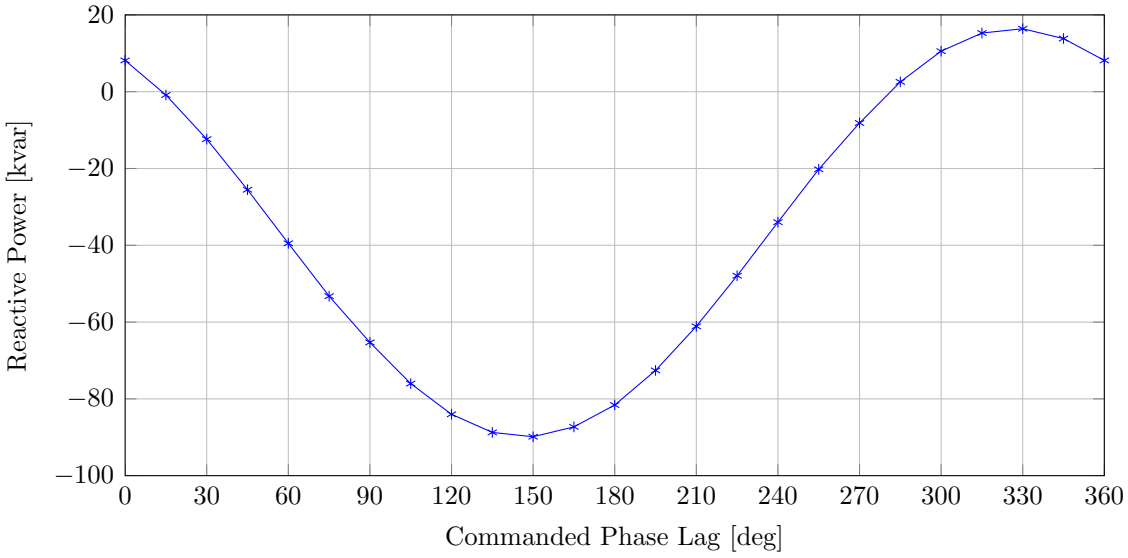

Figure 3-29: Reactive power entering the secondary bridge under different commanded phase lags.

3.3.1 Precise Power Flow in a Real Inductor

Initially, the process to obtain the classic power flow equation is going to be obtained. And then, applying the same procedure, the power flow equation considering the parasitic resistance will be extracted.

First of all, the current through the inductor should be obtained. In order to

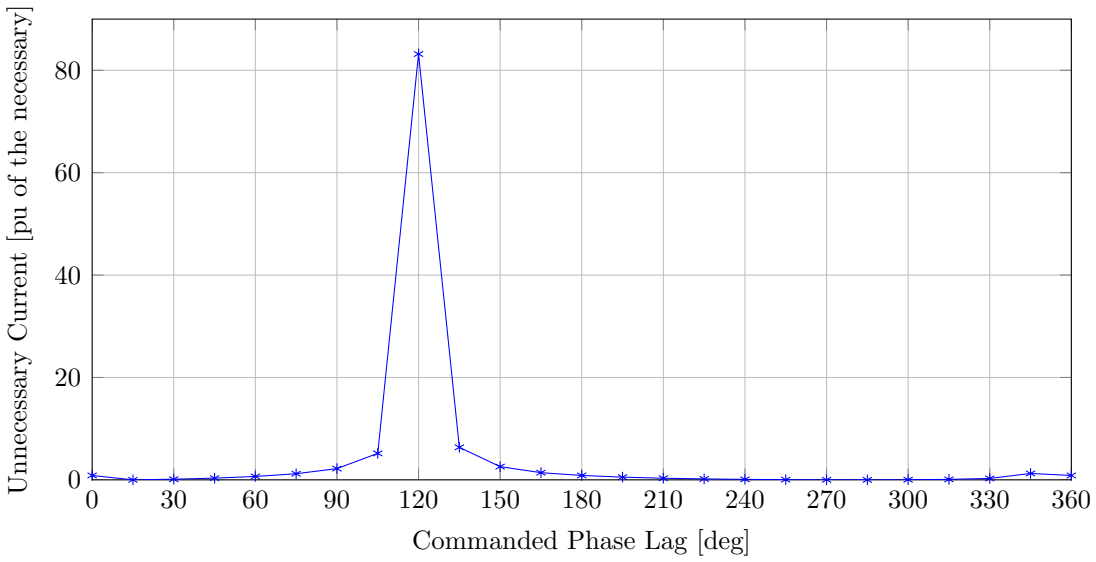

Figure 3-30: Amount of the current that is unnecessary with respect to the needed active current.

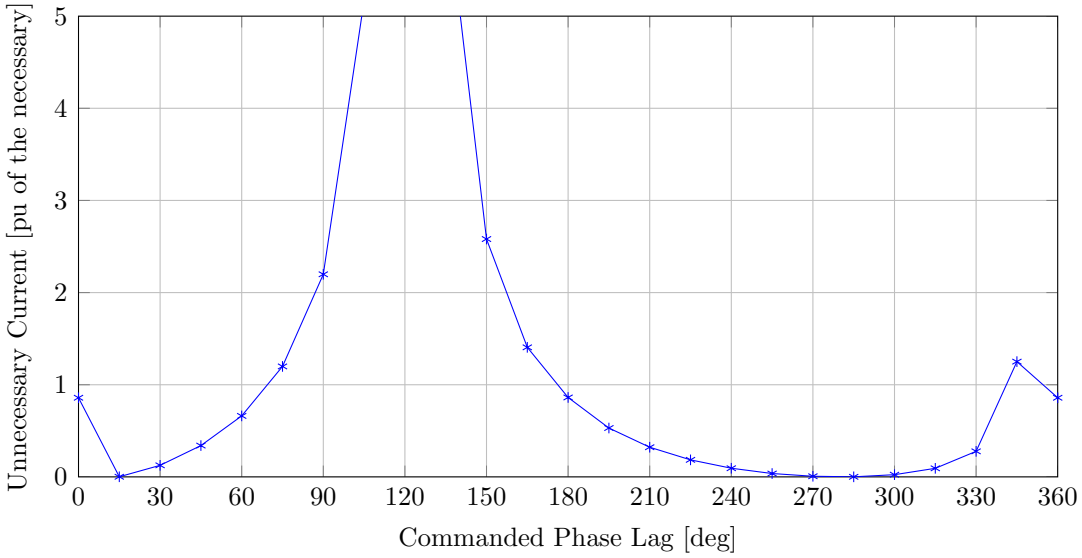

Figure 3-31: Zoom in the amount of the current that is unnecessary with respect to the needed active current.

do so, it has to be calculated the voltage across the inductor in terms of a function only dependant on one time variant trigonometric function (Eq. 3.4). Being $V_1 = \sqrt{2}V\sin(\omega t)$ and $V_2 = \sqrt{2}V\sin(\omega t - \delta)$:

$$V_{12} = V_1 - V_2 = 2\sqrt{2}V\sin(\delta/2)\cos(\omega t - \delta/2) \tag{3.4}$$

Now, the current (Eq. 3.5) is calculated by dividing the magnitude of the voltage by the impedance of the inductor and lagging the cosine $\pi/2$ radians. Then, the cosine is translated into a sine by adding a $\pi/2$ radians angle.

$$I_{12} = \frac{2\sqrt{2}V}{\omega L}\sin(\delta/2)\cos(\omega t - \delta/2 - \pi/2) = \frac{2\sqrt{2}V}{\omega L}\sin(\delta/2)\sin(\omega t - \delta/2)) \quad (3.5)$$

Once the current has been calculated, the obtention of the active power is straightforward. Just by multiplying the RMS values of the voltage and the currents by the cosine of the current angle, and applying trigonometric relations, the active power in the input terminal of the inductor (Eq. 3.6) and the output terminal (Eq. 3.7) are easily calculated. Obviously, considering this is the ideal equation without losses, both expressions have the same value.

$$P_1 = V_1 I_{12}\cos\phi = \frac{2V^2}{\omega L}\sin(\delta/2)\cos(\delta/2) = \frac{V^2}{\omega L}\sin(\delta) \quad (3.6)$$

$$P_2 = V_2 I_{12}\cos\phi = \frac{2V^2}{\omega L}\sin(\delta/2)\cos(-\delta/2) = \frac{V^2}{\omega L}\sin(\delta) \quad (3.7)$$

As expected, the calculated active power is the one presented in the previous chapter. Now, the power expression considering the additional losses given by the parasitic resistance will be derived. The approach is the same as before. As the voltages have the same value, the voltage across the inductor is also the same. But now the current expression changes (Eq. 3.8), as it depends on the value of both the resistance and the inductance of the real inductor.

$$\begin{aligned} I_{12} &= \frac{2\sqrt{2}V}{\sqrt{(\omega L)^2 + R^2}}\sin(\delta/2)\cos\left(\omega t - \delta/2 - \operatorname{atan}\left(\frac{\omega L}{R}\right)\right) = \\ &= \frac{2\sqrt{2}V}{\sqrt{(\omega L)^2 + R^2}}\sin(\delta/2)\sin\left(\omega t - \delta/2 - \operatorname{atan}\left(\frac{\omega L}{R}\right) + \pi/2\right) \end{aligned} \quad (3.8)$$

Now, the process to obtain the power is the same as before. But now, the sine and cosine have not the same angle, and so, they cannot be transformed into a single sine. That's why the powers (Eqs. 3.9 and 3.10) are a function of two different sinusoidal functions and do not follow a pure sine shape. It should be noticed that this effect is because $\text{atan}\left(\frac{\omega L}{R}\right) \neq \frac{\pi}{2}$. This equality is only true when $\frac{\omega L}{R} \uparrow\uparrow$.

$$P_1 = \frac{2V^2}{\sqrt{(\omega L)^2 + R^2}} \sin(\delta/2) \cos\left(\delta/2 + \text{atan}\left(\frac{\omega L}{R}\right) - \pi/2\right) \tag{3.9}$$

$$P_2 = \frac{2V^2}{\sqrt{(\omega L)^2 + R^2}} \sin(\delta/2) \cos\left(-\delta/2 + \text{atan}\left(\frac{\omega L}{R}\right) - \pi/2\right) \tag{3.10}$$

The goodness of this calculation can be seen in Fig. 3-32, where the power flowing through the primary and secondary bridges is plotted. The shape of the calculated power in the secondary bridge, despite of not being the same due to the presence of the transformer (the voltages are not the same) and the switching (square waves instead of sinusoidal), is quite close to the power shown in Fig. 3-28. For this reason, this equations can be assumed to be correct.

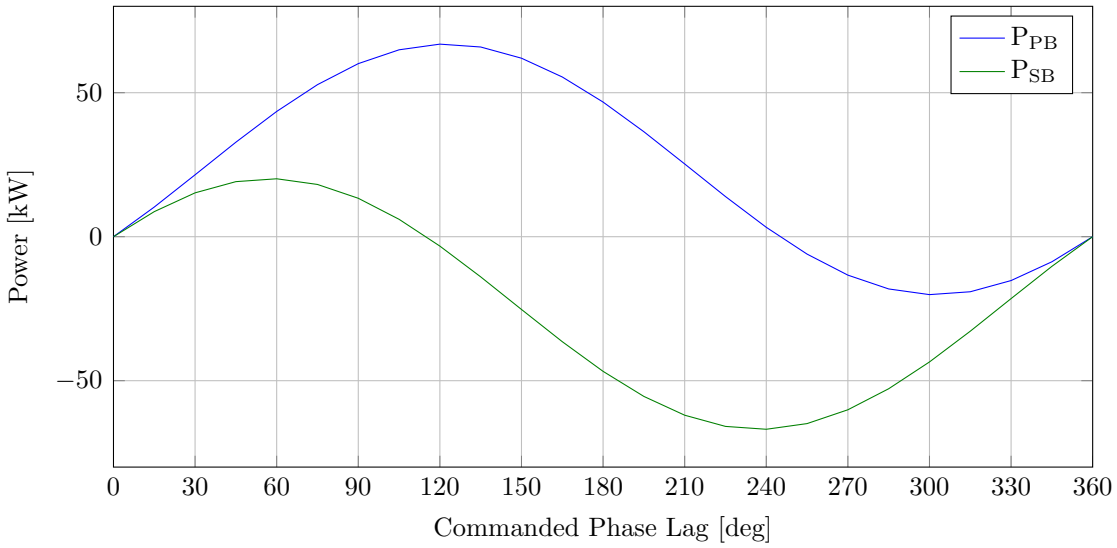

Figure 3-32: Calculated active power flowing through the primary and secondary bridge under different commanded phase lags.

3.4 Effect of the Dead Time in the Behaviour of the DAB

The dead time has a huge impact in the behaviour of the system compared to the ideal one (without dead time), as it can be seen in Figs. 3-33 and 3-34. This impact deviates the model from the calculated one, and thus, the response in the control won't be the one expected from the known model.

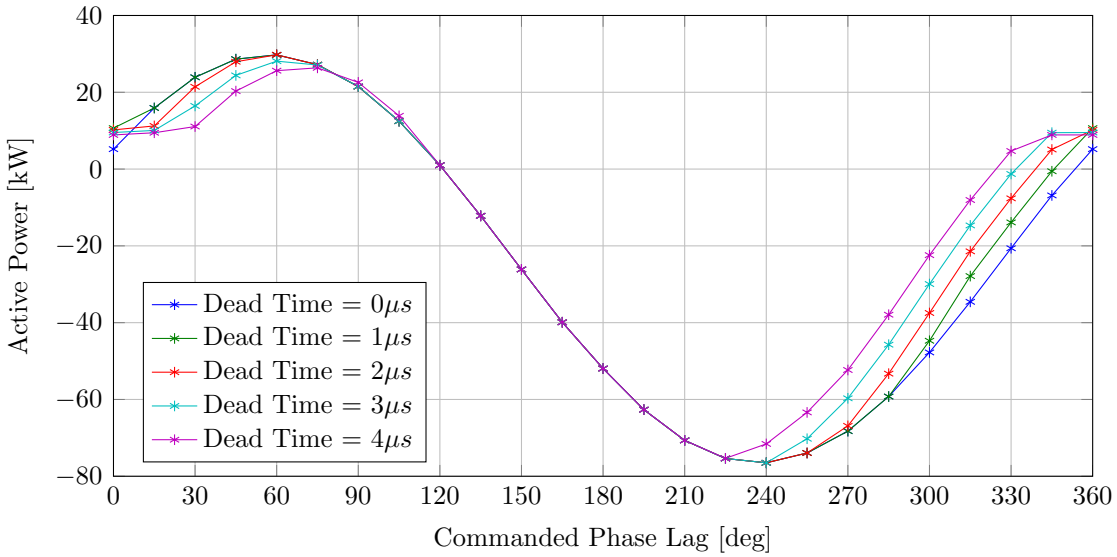

Figure 3-33: Active power entering the secondary bridge under different commanded phase lags with different dead times.

For this reason and based in the literature [13], a function to estimate the effect of the dead time depending on the operating point and a method for compensating its effect is now explained.

3.4.1 Dead Time Compensation

First of all, an internal variable δ_s is calculated. This variable represents the time, in terms of angle, when the current needs to reach zero in the inductor. In Eq. 3.11 δ_s is shown for the case when the primary bridge leads the secondary. In Eq. 3.12 it is calculated for the opposite case.

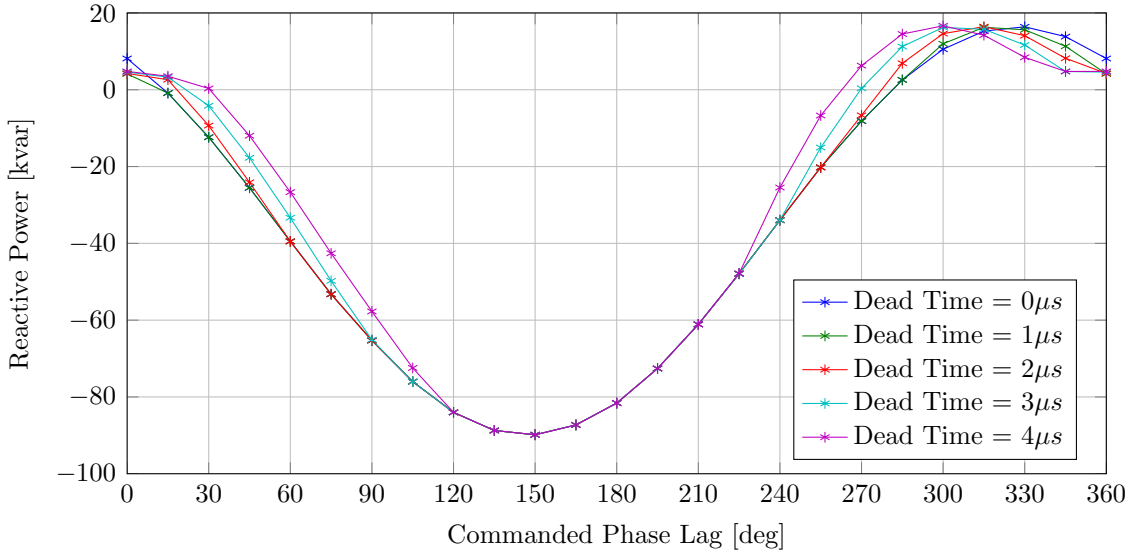

Figure 3-34: Reactive power entering the secondary bridge under different commanded phase lags with different dead times.

$$\delta_s = \delta_c - \frac{V_H - V_L}{V_H}\frac{\pi}{2} - \frac{V_L}{V_H}\delta_{DT} \tag{3.11}$$

$$\delta_s = -\delta_c + \frac{V_H - V_L}{V_H}\frac{\pi}{2} \tag{3.12}$$

Once δ_s is calculated, the estimation of the effect of the dead time, δ_{db}, is calculated based on this value, which is compared with the dead time, and selected as a function of the voltages in Tab. 3.5.

The value of δ_{db} is now represented in several plots. In this case, as the value of $V_{in} = V_{out}$, only one row of the table is necessary. In Figs. 3-35 and 3-36, δ_{db} is obtained as a function of the dead time (in μs) and the commanded phase lags between the bridges, δ_c. In Figs. 3-37 and 3-38, the effect is represented in the same way, but the dead time is represented in degrees, using the expression $\delta_{DT} = t_{DT} \cdot f \cdot 360°$. Finally, in Fig. 3-39, a look from the $\delta_{db} - \delta_c$ view is shown to simplify the understanding of the plots.

Table 3.5: Dead Time Compensation Function [13].

	$V_{in} > \frac{N_p}{N_s} V_{out}$		$V_{in} < \frac{N_p}{N_s} V_{out}$	
	δ_s	δ_{db}	δ_s	δ_{db}
Primary Bridge	$\delta_s > \delta_{DT}$	0	$\delta_s > \delta_{DT}$	$-\delta_{DT}$
Leads	$0 < \delta_s < \delta_{DT}$	$\delta_{DT} - \delta_s$	$0 < \delta_s < \delta_{DT}$	$-\delta_s$
Secondary Bridge	$\delta_s < 0$	δ_{DT}	$\delta_s < 0$	0
Primary Bridge	$\delta_s > \delta_{DT}$	δ_{DT}	$\delta_s > \delta_{DT}$	0
Lags	$0 < \delta_s < \delta_{DT}$	δ_s	$0 < \delta_s < \delta_{DT}$	$-\delta_{DT} + \delta_s$
Secondary Bridge	$\delta_s < 0$	0	$\delta_s < 0$	$-\delta_{DT}$

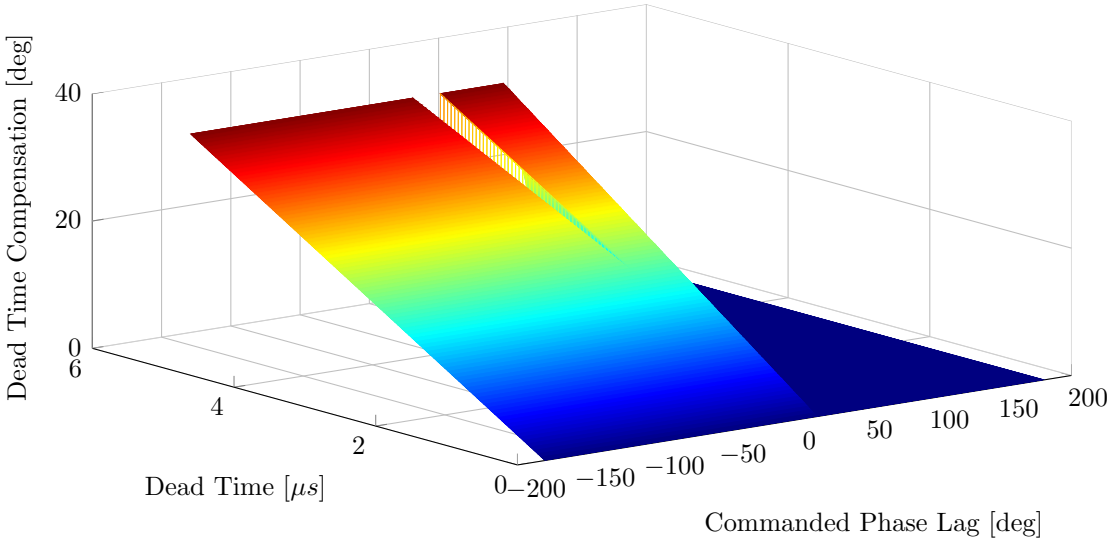

Figure 3-35: Dead time compensation for different dead times (measured in μs) and angles of commanded phase lag.

3.5 DAB Control

In this last section, the proposed control strategy is explained. In the literature, different types of control strategies are analysed. The most used are:

1. Control of the current in the inductor.

2. Control of the output DC capacitor voltage.

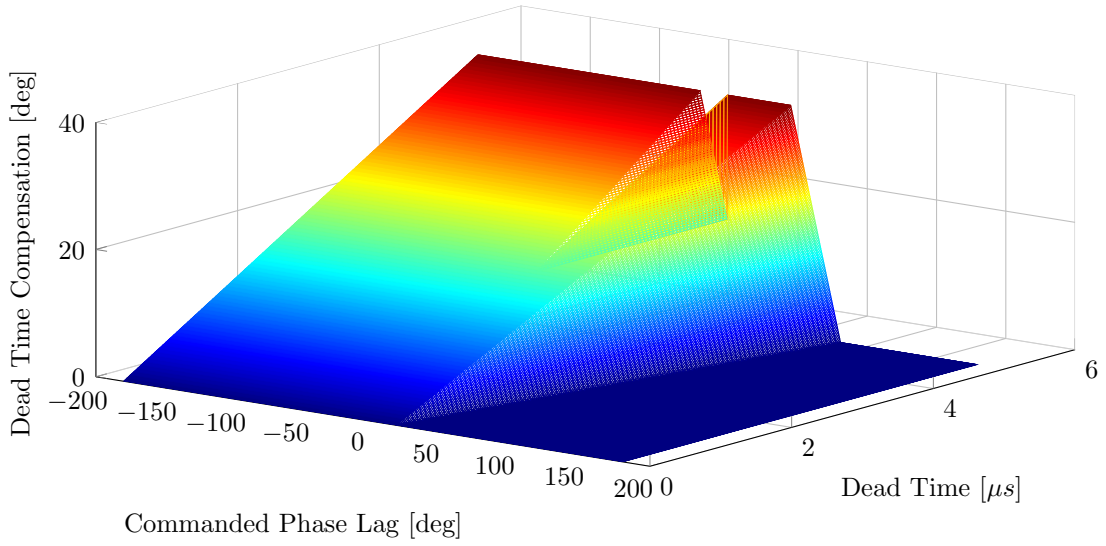

Figure 3-36: Dead time compensation for different dead times (measured in μs) and angles of commanded phase lag.

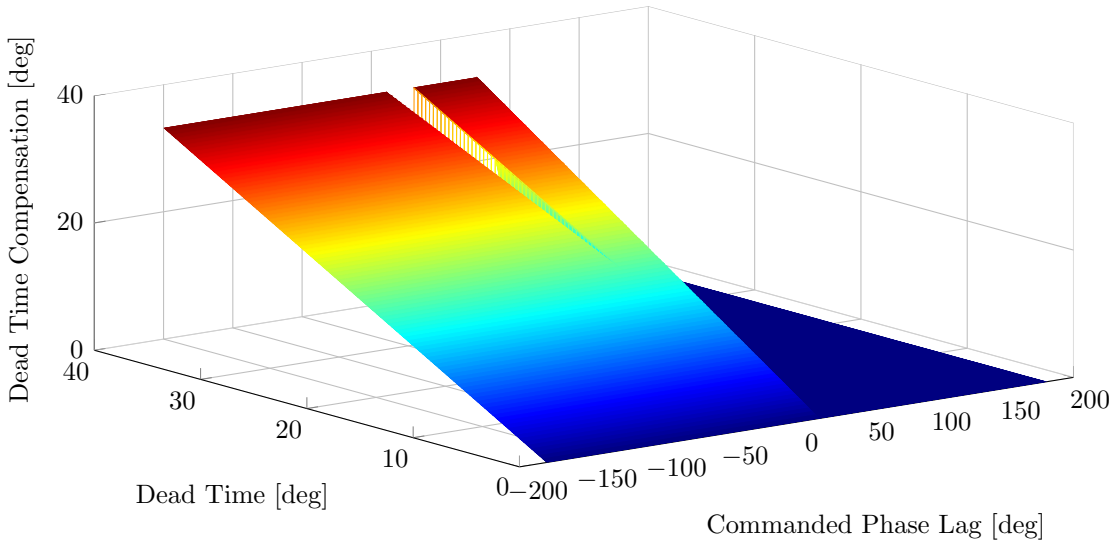

Figure 3-37: Dead time compensation for different dead times (measured in degrees) and angles of commanded phase lag.

In this thesis, due to its simplicity, the selected control strategy was the second one. However, in future work, a comparison between both methods should be done, checking which is better for each application and how each control faces the problems of reactive power and dead time effect.

The selected control strategy power topology is shown in Fig. 3-40, where the only variable that needs to be measured for control purposes is the output DC capacitor

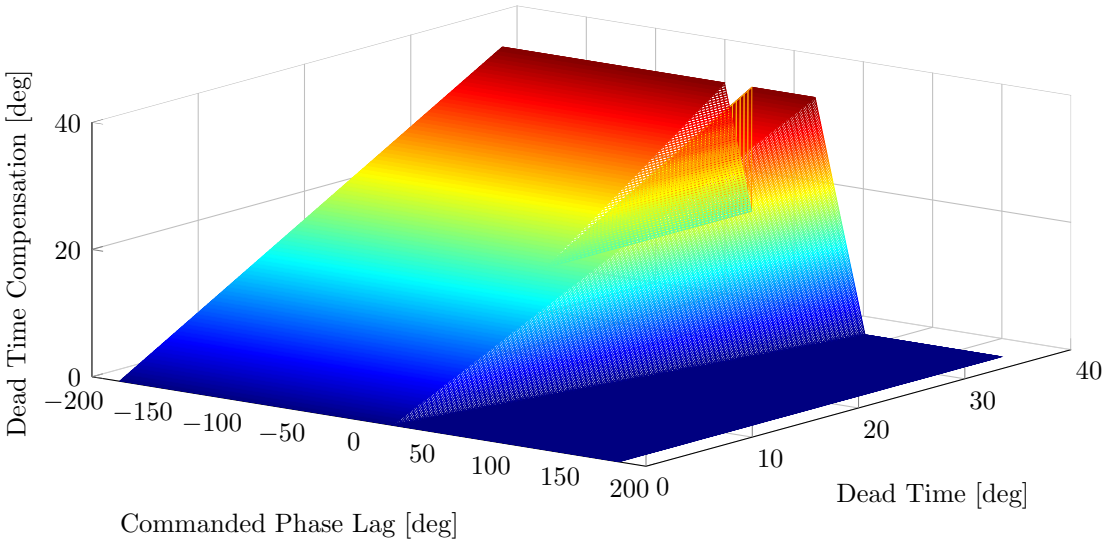

Figure 3-38: Dead time compensation for different dead times (measured in degrees) and angles of commanded phase lag.

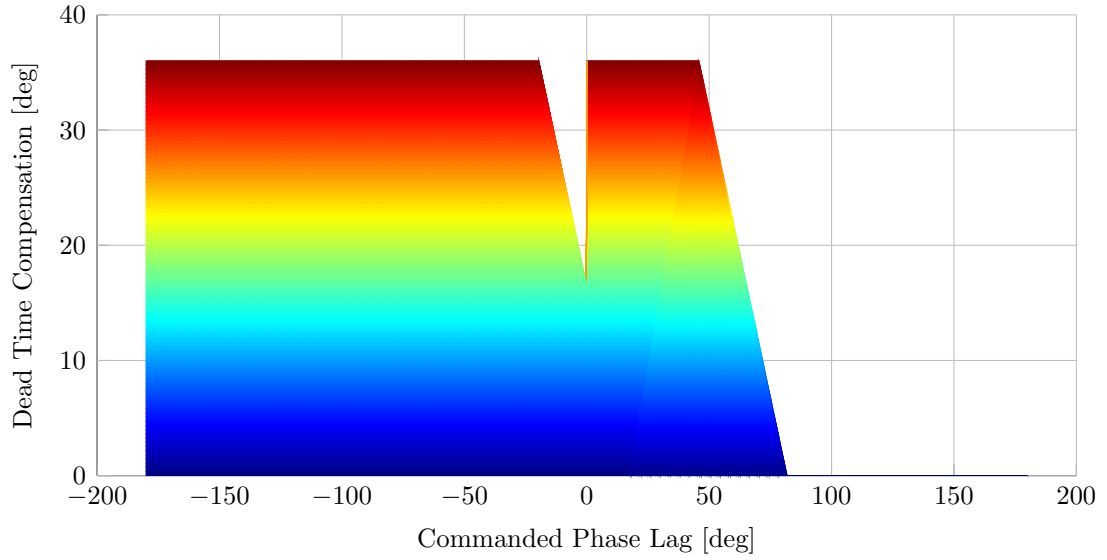

Figure 3-39: Dead time compensation for different dead times and angles of commanded phase lag.

voltage. Here, it is supposed that the primary bridge is fed by a power source and the secondary bridge will charge the output capacitor. The initial block diagram of the control is shown in Fig. 3-41. The power flow will be controlled by maintaining the output capacitor voltage constant, this means that the capacitor gives the demanded power and the DAB tries to match this power.

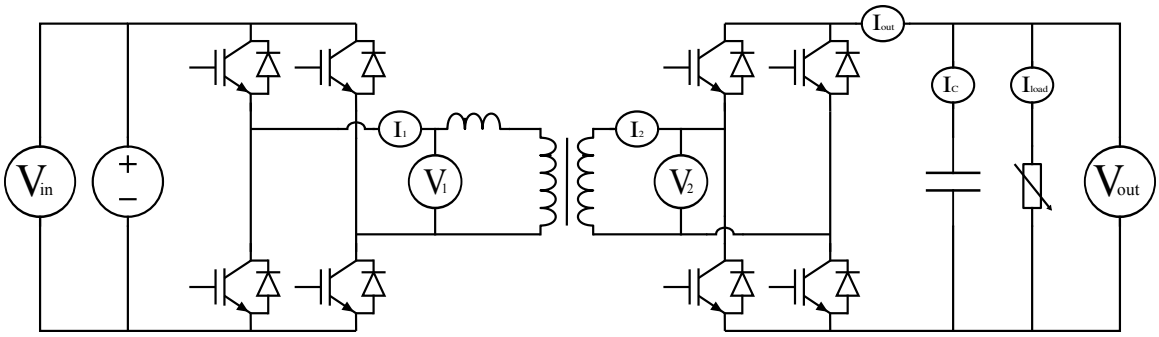

Figure 3-40: Power topology for the control of a dual active bridge.

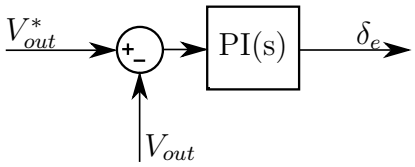

Figure 3-41: Initial control scheme.

The problem of the previous scheme is the one mentioned before, the dead time will affect the response of the system to the commanded phase lag. To solve this, the dead time effect is subtracted from the commanded phase, as shown in Fig. 3-42. But, in with this control, also the input voltage should be measured, as it cannot be assumed to be a perfectly constant DC voltage as the input power supply (rectifier, boost converter, etc...) can make the voltage to oscillate.

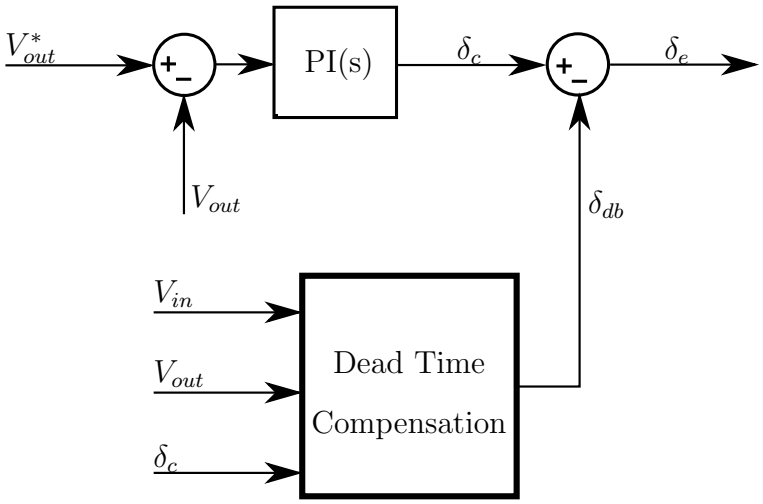

Figure 3-42: Final control scheme with dead time compensation.

Chapter 4

Simulation Results

In this chapter, the results of the simulations covered to check the behaviour of the DAB system in closed loop will be shown and explained, comparing the two different controls (with and without dead time compensation) proposed in the previous chapter.

All the simulations have been done using MATLAB and Simulink. In order to simulate the power elements, such as transformers, passive elements, power electronics... the SimPowerSystems toolbox was used. The remaining used blocks were from the basic Simulink library.

The implementation of the electronic converter power topology is shown in Fig. 4-1. The reason why the primary bridge is connected to the secondary of the transformer and the secondary bridge to the primary of the transformer is only a matter of what has been named as primary and secondary of the transformer, as explained in the previous chapter.

In Fig. 4-1, the following measurements were done to plot the figures that are going to be shown in the following pages:

1. Input and output DC voltages

2. Voltages applied to the primary and the secondary of the transformer

3. Current flowing through the primary and secondary bridges (or the opposite sides of the transformer)

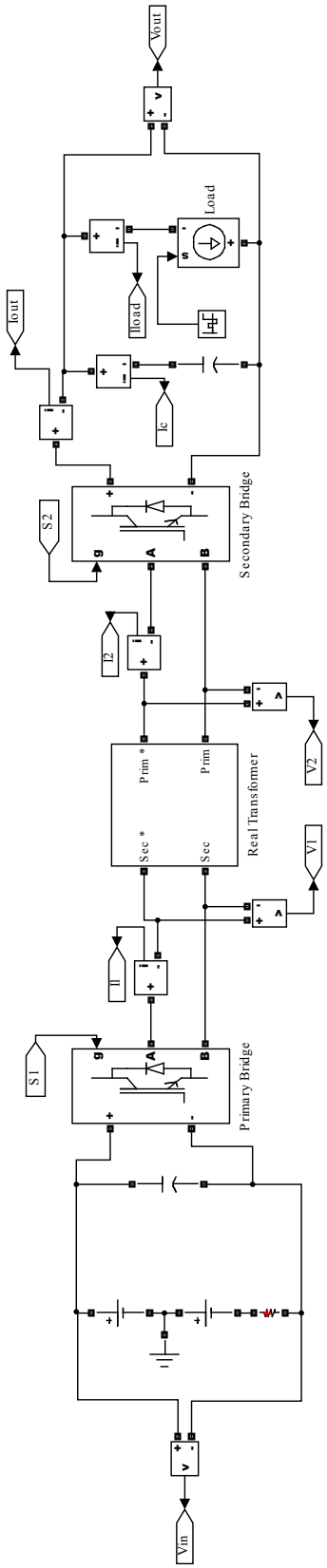

Figure 4-1: Dual Active Bridge scheme used in the simulations.

4. Currents in the output DC link: current from the bridge, capacitor current and load current

The selected parameters for the PI controllers of both schemes: with and without dead time compensation, based on the tuning given in the literature [13], are listed in Tab. 4.1.

Table 4.1: PI parameters.

Parameter	Value
K_p	$50 \cdot 10^{-2}$
K_i	10^3

The performance of both schemes will be analysed during a transient in the load, changing from different positive and negative values every $15ms$, will be analysed. The results are depicted by plotting the evolution of different variables during the transient

4.1 DAB Control without Dead Time Compensation

This first section will cover the simulations of the DAB converter without including the compensation of the dead time.

In Fig. 4-2 the average of the currents in the output DC bus are shown. As it can be seen, the current of the load, I_{load}, is always equal to the sum of the current from the secondary bridge, I_{out}, and the capacitor current, I_C, as should be expected from the Kirchhoff's law. It is also clear in the plot that, once the transient has finished, the current in the capacitor is kept constant around 0.

The output DC capacitor voltage is shown in Fig. 4-3. Here, a noticeable overshoot peak of more than 20% appears in the first part of the plot. This peak may be dangerous to the capacitor depending on how close the working DC voltage is from the maximum acceptable voltage for the capacitor.

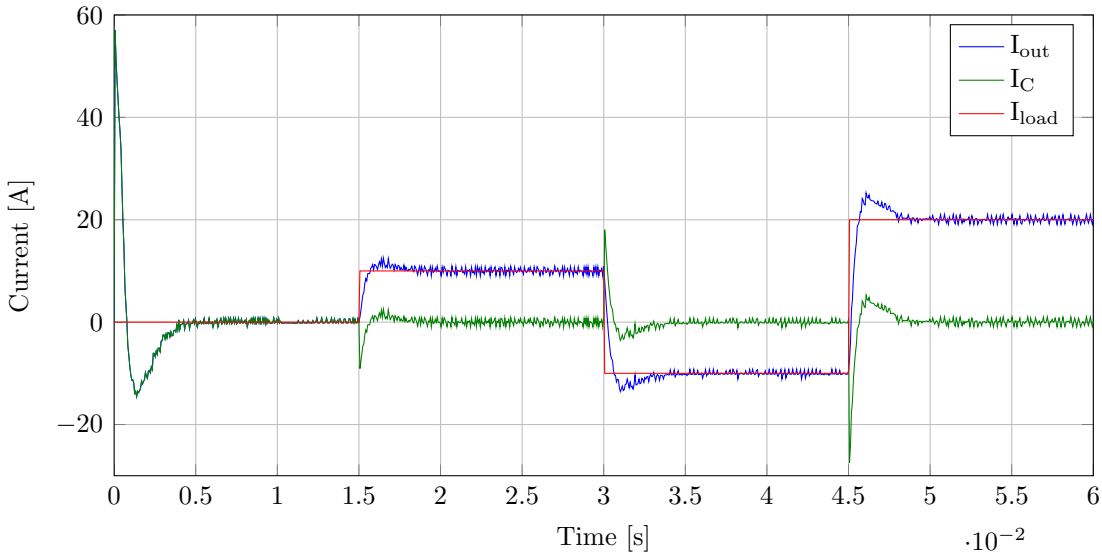

Figure 4-2: Average of the currents in the DC output under a varying load situation in closed loop control: current from the bridge, current in the capacitor and load current.

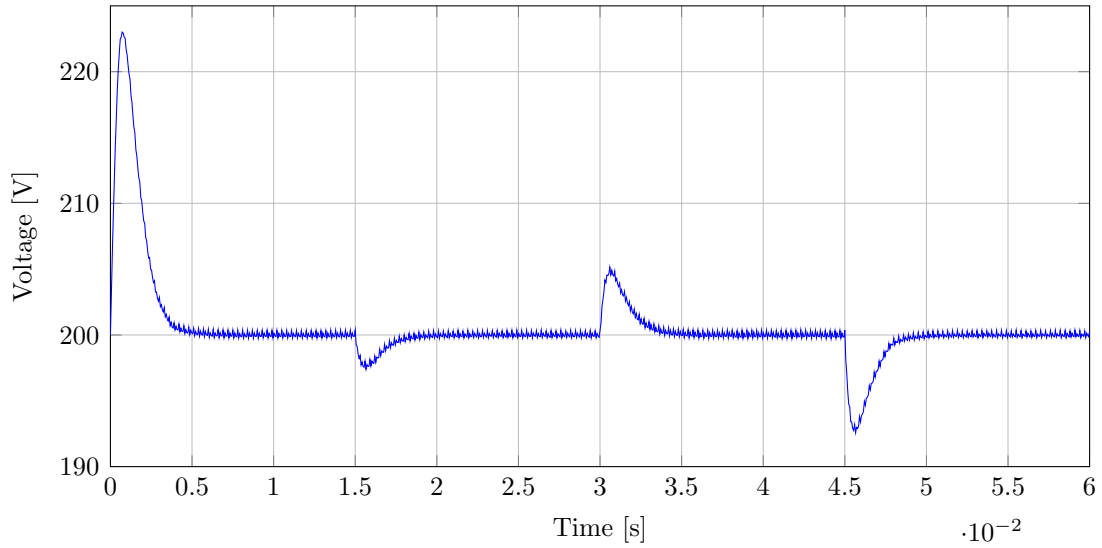

Figure 4-3: Output capacitor voltage under a varying load situation in closed loop control.

In Fig. 4-4, the value of the commanded phase lag applied between the square wave voltages of the primary and secondary bridges is represented. As it can be seen, excepting the initial response, the value of the phase lag is relatively high in magnitude. The low values in the first part may be the responsible of the initial peak, because is with low angles when the dead time effect is greater, as it has been shown

in the previous chapter.

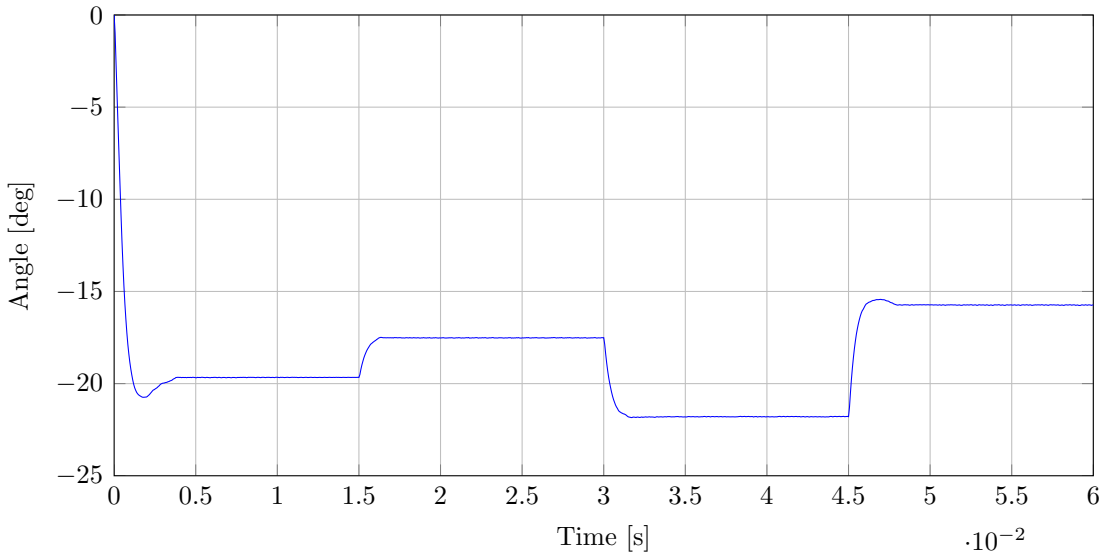

Figure 4-4: Phase lag commanded by the PI controller under a varying load situation.

In Figs. 4-5 and 4-6 the active and reactive power through the primary and secondary bridges are plotted.

As shown, the shape of the current from the secondary bridge in Fig. 4-2, I_{out}, is quite close to the shape of the active power through the secondary bridge. The reason why they are not simply proportional is because the power calculations (active and reactive) are extracted from a fundamental power computer block, and so the power is not the actual power of the square wave voltage and corresponding current (formed by a repeating sequence of different exponentials), and also because of the non-constant output DC voltage.

As it has be mentioned throughout this thesis, the presence of reactive power has no benefit. And, as seen in the plot, the reactive power is always in a range of 2 times the active power. This value is extremely high and will mean losses in every power device.

In both figures, the difference between the primary and secondary bridges powers is due to the power consumption of the transformer.

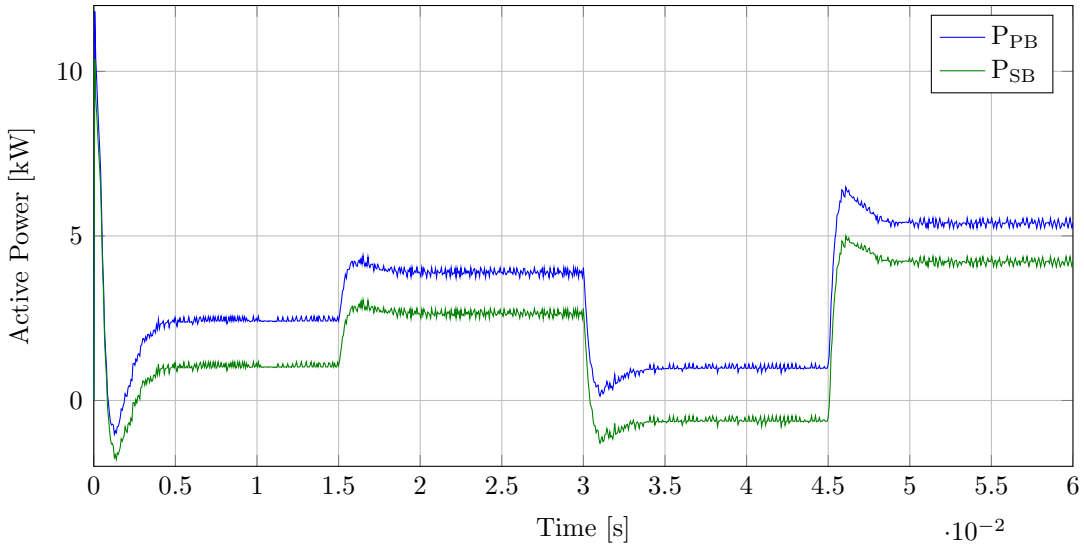

Figure 4-5: Fundamental active powers flowing through the primary and secondary bridges under a varying load situation in closed loop control.

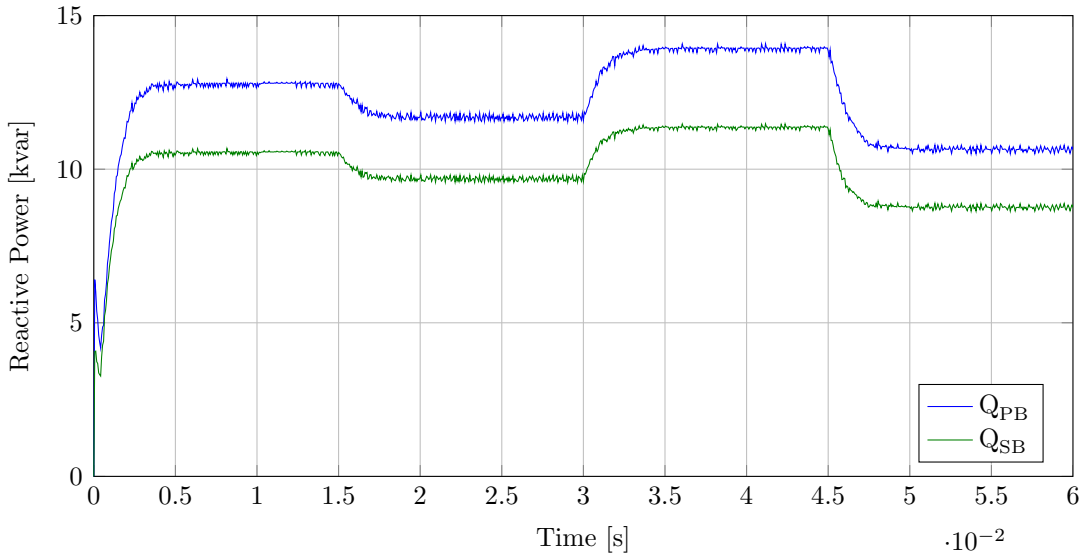

Figure 4-6: Fundamental reactive powers flowing through the primary and secondary bridges under a varying load situation in closed loop control.

4.2 DAB Control with Dead Time Compensation

This section will cover the simulation of the DAB converter compensating the effect of the dead time and the comparison with the previous ones.

In Fig. 4-7 appears the average of the currents in the output DC bus. In this case, the response is quite similar to 4-2, excepting the initial current, due to the

compensation.

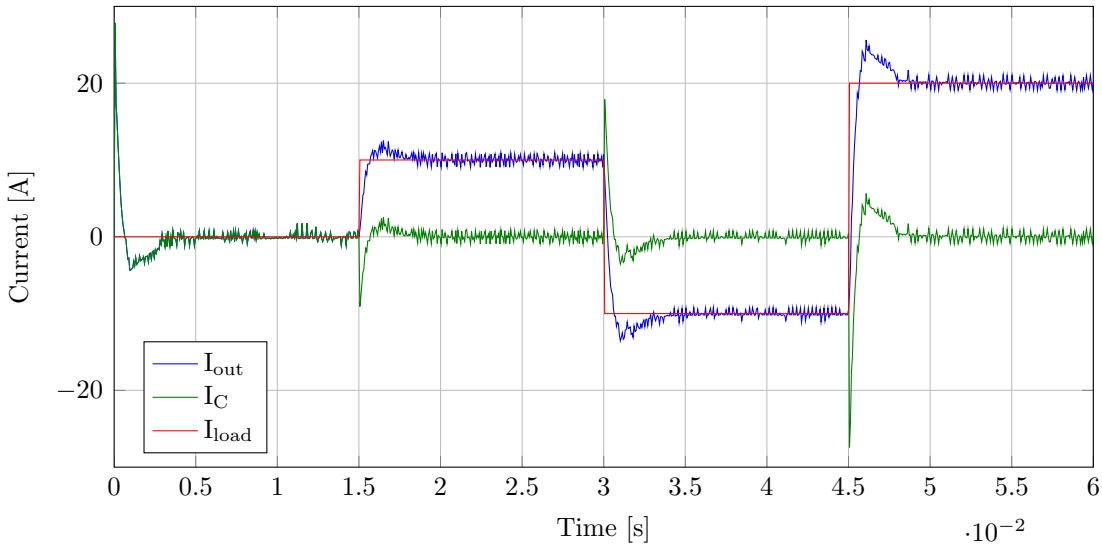

Figure 4-7: Average of the currents in the DC output under a varying load situation in closed loop control with dead time compensation: current from the bridge, current in the capacitor and load current.

The output DC capacitor voltage is shown in Fig. 4-8. Here, the overshoot in the first part of the plot in Fig. 4-3 disappears. This is due to the compensation of the dead time effect. However, the other peaks are almost the same than in the previous plot. This is because these peaks are caused by the change in the load, and not by the dead time.

In Fig. 4-9, the values of the different angles are plotted: the phase lag applied between the square wave voltages of the primary and secondary bridges, δ_e; the phase lag commanded by the PI controller, δ_c; the estimated dead time effect that is subtracted from the commanded phase lag, δ_{db}, and the internal variable, used to calculate δ_{db}, δ_s. The addition of δ_{db} is the responsible of a better response in the initial part of the simulation in 4-8.

In Figs. 4-10 and 4-11 the active and reactive power through the primary and secondary bridges are plotted. Once again, the values are quite close to the ones in Figs. 4-5 and 4-6. This is because, even with dead time compensation, the load is the same and so the powers should also be the same.

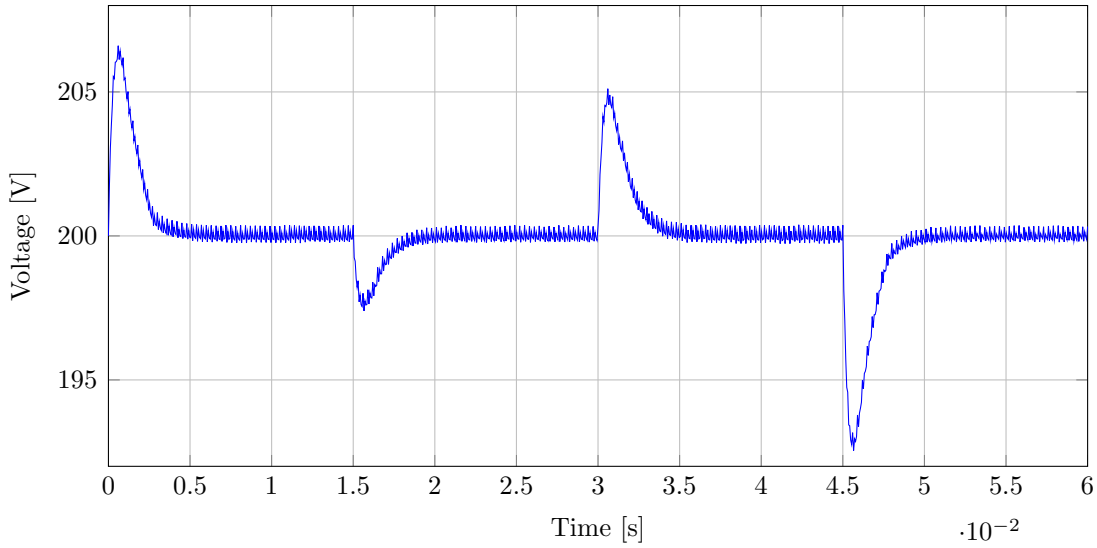

Figure 4-8: Output capacitor voltage under a varying load situation in closed loop control with dead time compensation.

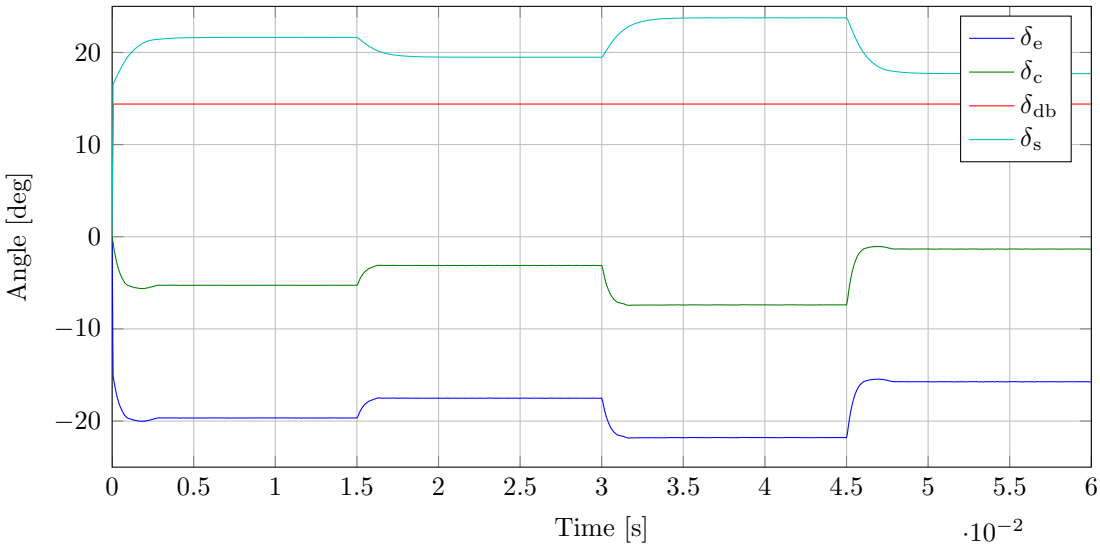

Figure 4-9: Phase lag commanded by the PI controller without dead time effect, phase lag commanded by the PI controller with dead time effect, dead time effect and internal variable δ_s under a varying load situation with dead time compensation.

4.3 Conclusions

As a summary, it can be concluded that the response of the DAB to load changes is quite fast, achieving steady state, approximately, in $5ms$, 1/4 of a $50Hz$ wave cycle. This makes the DAB a quite versatile converter.

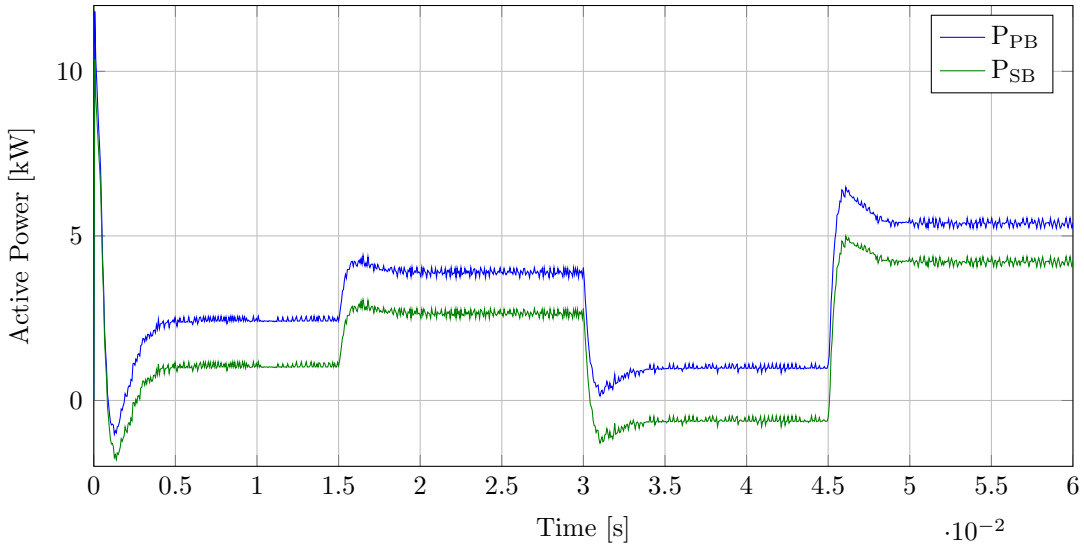

Figure 4-10: Fundamental active powers flowing through the primary and secondary bridges under a varying load situation in closed loop control with dead time compensation.

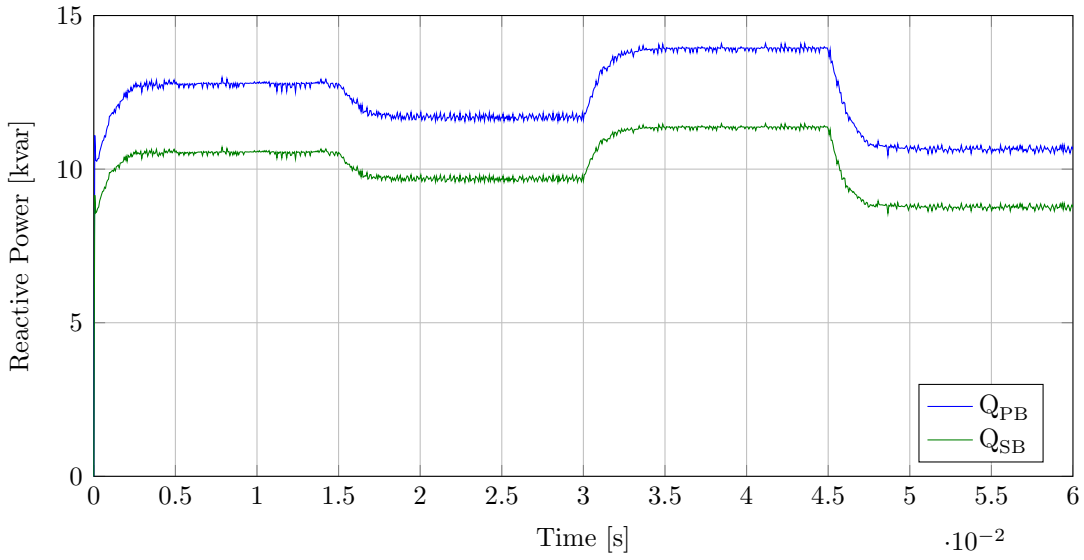

Figure 4-11: Fundamental reactive powers flowing through the primary and secondary bridges under a varying load situation in closed loop control with dead time compensation.

It is also important to mention that, once the dead time is compensated, the response of the converter is improved, specially with low phase lags (low powers).

Finally, it should be also pointed that the amount of reactive power exchanged between the primary and secondary is very big compared with the active power. A

reactive power around 10% could be acceptable, but being twice the value of the reactive power, this is a problem that should be solved in future work.

4.3.1 Experimental Implementation

In order to try to understand much deeper the operation of the DAB, one physical prototype was started. The main components of this implementation are:

1. The Himag planar transformer, modelled in chapter 3.
2. Two Guasch three phase inverters, using only two legs to control the DAB and leaving the third one free. This last leg could be used to act as a variable load with a resistor. This inverters have internal measurements of the DC voltage and currents in each leg.
3. Some power resistors acting as loads and hysteresis protections for the DC links.
4. A Texas Instruments TMS320F28335 digital signal controller where all the control and modulations are implemented.
5. Three interface boards, two of them equal, used to link the inputs (gate signals) and outputs (measurements) of the inverters with de DSC.

Because of problems with time and with the final implementation, this built prototype could not be used to run the DAB, neither in open loop operation nor in closed loop. However, as the converter is already built, it could be used for the future work that is going to be presented in chapter 5.

Chapter 5

Conclusions and Future Work

In this chapter a set of conclusions based on all the work done during the development of this thesis are presented. And also, looking forward, some possible work that should be done in the future is included.

5.1 Conclusions

From this work, the most important conclusions that could be gathered, based on the literature, calculation, simulations and experimentation, are:

DAB fast response: As it could be seen in the simulations, the DAB is a quite fast device, matching the power to the required one in tenths of a second. With this characteristic, the DAB is a great candidate to be a power converter in future smart grids and micro grids, being able to keep the equality of generation and demand almost instantaneously.

Dead time problem: The dead time, mandatory in every power converter with two or more switches in a leg in parallel with a voltage source or DC link to avoid short circuits, can affect strongly the behaviour of the converter, especially with low power ratios, when the phase angle is low. The main effect is that, when the commanded angle is low, and that means that the power flow will also be low, the effective angle applied to the converter will be distorted, flowing less

power than the expected at that demanded angle. The compensation used in this thesis is a good solution in order to avoid the enumerated problems.

Unacceptable reactive power: The amount of reactive power that is flowing through the DAB is quite high compared with the active power. But, however, the percentage of this reactive power that is being consumed by the inductor is relatively low. The problem of the reactive power is maximum, with this transformer, at 120°, where the active power is near 0 and the reactive power near its maximum value, and minimum around 15° and 270°, where the active power is high and the reactive close to 0. However, as the reactive power is related with the active, as both depend on the phase lag, and the active power is fixed by the load, the reactive power will also be fixed by the load conditions. For this reason, this extra reactive power should be minimized or even cancelled.

Losses in the transformer: As it could be seen in chapter 3, the effect of the resistive part of the inductor (transformer) deviates the behaviour of the power flow from what is commonly known in distribution systems. The usage of a transformer with lower losses may result in a more ideal behaviour of the system.

5.2 Future Work

Once the work of this thesis has finished, the information acquired during its development could be used for going further in the investigation of the DAB. Several ways of improvement are presented in the following points:

- Different modulation strategies should be tested. PWM could also be used, in order to reduce the harmonics in the current. The main problems of the PWM are two: as the frequency of the transformer is already high frequency, the switching frequency should be higher, and this may result in high losses in the switches, especially if the voltage is increased.

- The control of the DAB can be improved, by a better tuning, or a more complex control strategy including load feedforward, adaptive PI controller and similar

features. A different control could also be tested, like an inductor current control. This control may be easier with the PWM modulation, as the currents shape will be closer to a sinusoidal.

- The reactive power through the converter should be minimized. In order to do so, based in the literature, a new control using two phases (between bridges and between legs of a bridge) could be used to improve the efficiency of the converter.

- The started prototype must be finished and some experimental results obtained in order to verify the implemented model.

- Once the prototype is fully functional, another prototype with higher ratings in power and voltage, closer to the rating of the planar transformer ($10kW$).

- Finally, a high power and high voltage prototype could be designed to operate in conditions closer to what is expected in a power converter used in a micro grid.

- Going further in the research, the number of windings of the transformer could be increased, building a triple active bridge, TAB. With this converter, a renewable power source could be added and the power flow between that source, the energy storage system and the grid controlled.

Appendix A

MatLab Code with the Dead Time Effect Estimation

```
function [d_db, d_s] = fcn(Vin, Vout, d_c, tdt, f, Npri_Nsec)
%#codegen

d_DT=tdt*f*360;
Vh=Vin;
Vl=Vout/Npri_Nsec;

if (d_c>0) && (d_c<180) || (d_c>-360) && (d_c<-180)

    d_s=d_c-(Vh-Vl)/Vh*90-Vl/Vh*d_DT;

    if Vin>Vout/Npri_Nsec

        if d_s>d_DT

            d_db=0;

        elseif (0<=d_s) && (d_s<d_DT)

```

```
20              d_db=d_DT-d_s;
21
22          else
23
24              d_db=d_DT;
25
26          end
27
28      else
29          if d_s>d_DT
30
31              d_db=-d_DT;
32
33          elseif (0<=d_s) && (d_s<d_DT)
34
35              d_db=-d_s;
36
37          else
38
39              d_db=0;
40
41          end
42      end
43  else
44
45      d_s=-d_c+(Vh-Vl)/Vh*90;
46
47      if Vin>Vout/Npri_Nsec
48
49          if d_s>d_DT
50
51              d_db=d_DT;
```

```
52
53          elseif (0<=d_s) && (d_s<d_DT)
54
55              d_db=d_s;
56
57          else
58
59              d_db=0;
60
61          end
62
63      else
64          if d_s>d_DT
65
66              d_db=0;
67
68          elseif (0<=d_s) && (d_s<d_DT)
69
70              d_db=-d_DT+d_s;
71
72          else
73
74              d_db=-d_DT;
75
76          end
77      end
78  end
```

Code A.1: AMatLab Code with the Dead Time Effect Estimation.

Appendix B

Planar Transformers Measurements

When doing the estimation of the parameters of the transformers, the measurements were done in two identical transformers, both connecting the primary side to the impedance analyser and the secondary side.

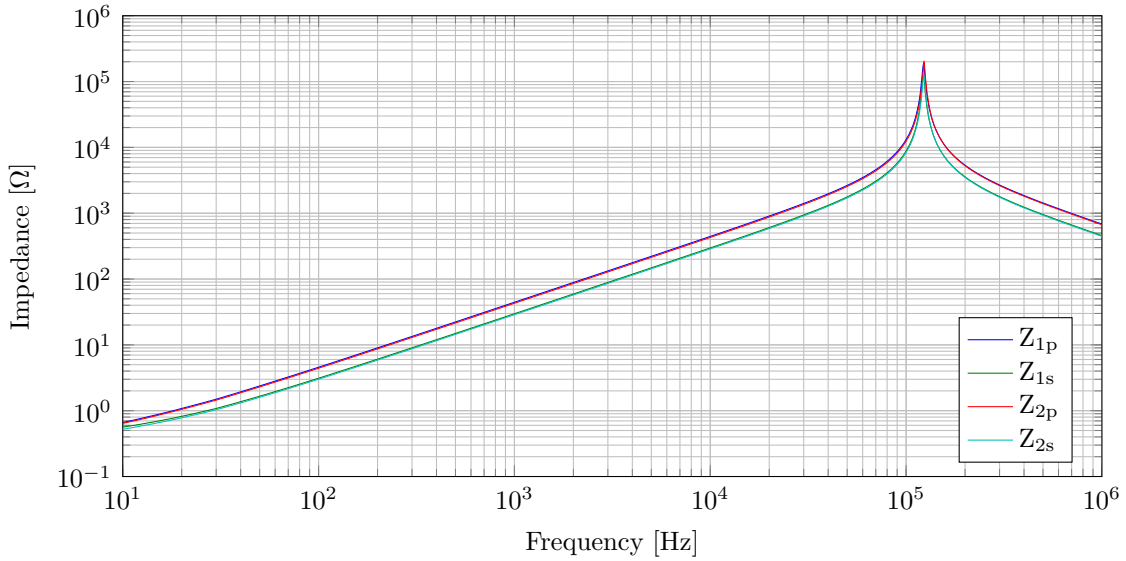

Figure B-1: Transformer impedance under a no-load test measured in the primary and secondary of both transformers.

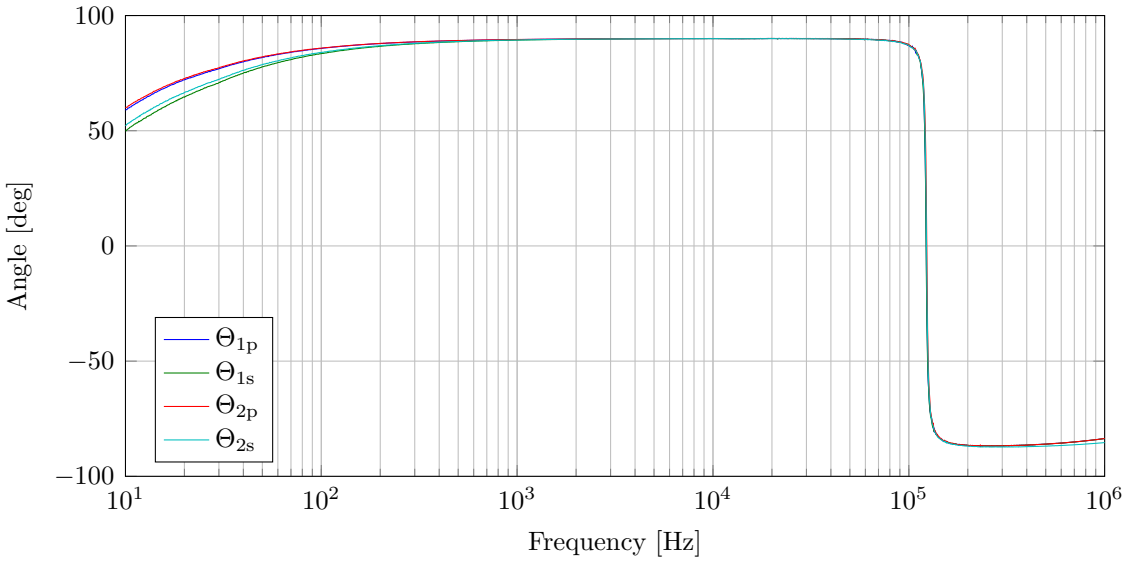

Figure B-2: Transformer impedance angle under a no-load test measured in the primary and secondary of both transformers.

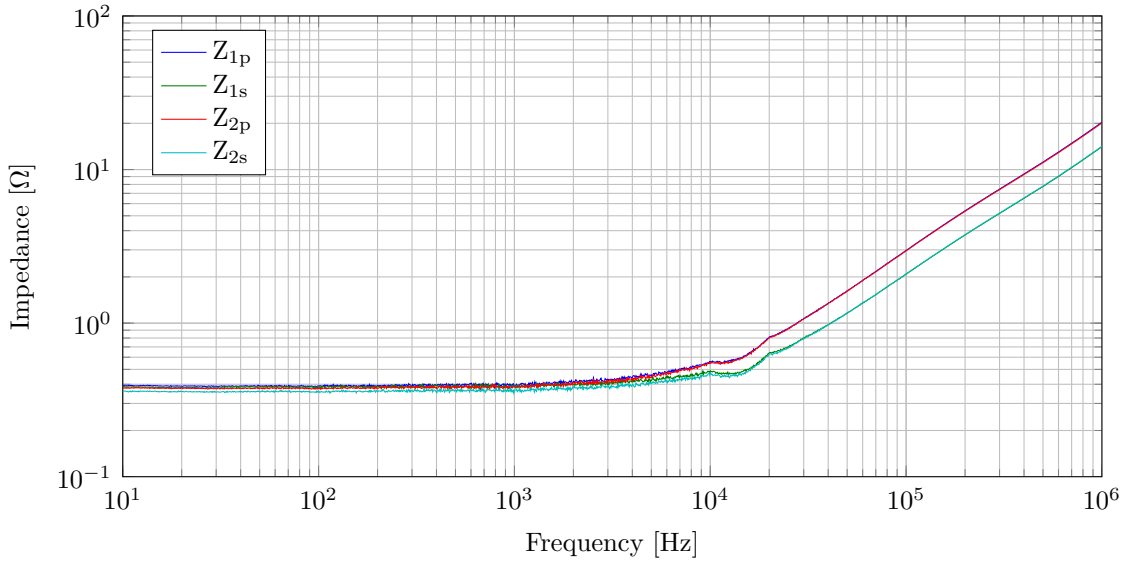

Figure B-3: Transformer impedance under a short circuit test measured in the primary and secondary of both transformers.

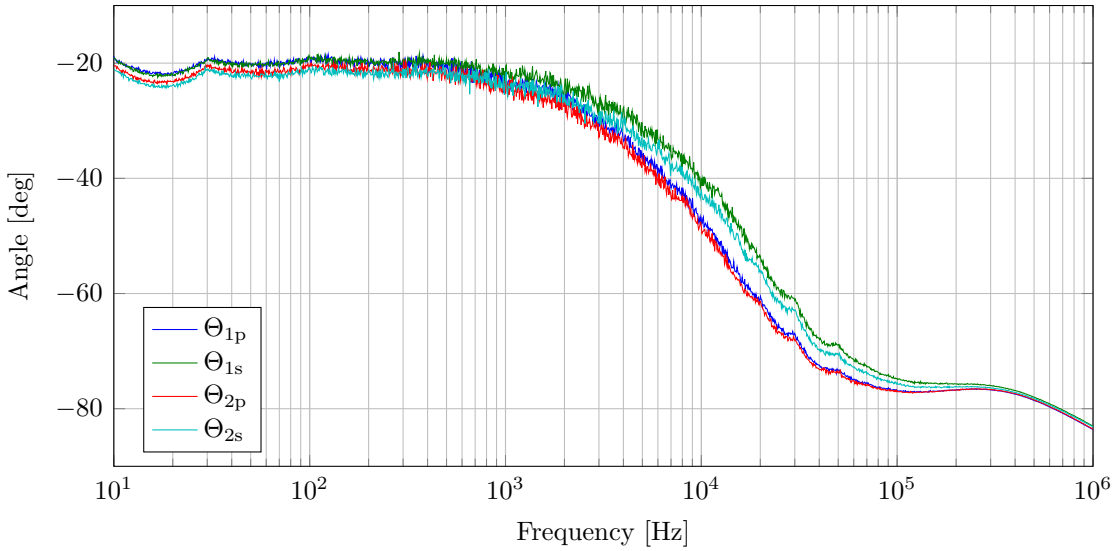

Figure B-4: Transformer impedance angle under a short circuit test measured in the primary and secondary of both transformers.

Bibliography

[1] Hua Bai and C. Mi. Eliminate Reactive Power and Increase System Efficiency of Isolated Bidirectional Dual-Active-Bridge DC-DC Converters Using Novel Dual-Phase-Shift Control. *IEEE Transactions on Power Electronics*, 23(6):2905–2914, November 2008.

[2] L. Chen, A. Amirahmadi, Q. Zhang, N. Kutkut, and I. Batarseh. Design and Implementation of Three-Phase Two-Stage Grid-Connected Module Integrated Converter. *IEEE Transactions on Power Electronics*, 29(8):3881–3892, August 2014.

[3] R.W. De Doncker, D.M. Divan, and M.H. Kheraluwala. A three-phase soft-switched high power density DC/DC converter for high power applications. pages 796–805. IEEE, 1988.

[4] S.P. Engel, N. Soltau, H. Stagge, and R.W. De Doncker. Improved Instantaneous Current Control for High-Power Three-Phase Dual-Active Bridge DC-DC Converters. *IEEE Transactions on Power Electronics*, 29(8):4067–4077, August 2014.

[5] J. Everts, F. Krismer, J. Van den Keybus, J. Driesen, and J.W. Kolar. Optimal ZVS Modulation of Single-Phase Single-Stage Bidirectional DAB AC-DC Converters. *IEEE Transactions on Power Electronics*, 29(8):3954–3970, August 2014.

[6] P. Jain, M. Pahlevaninezhad, S. Pan, and J. Drobnik. A Review of High-Frequency Power Distribution Systems: For Space, Telecommunication, and Computer Applications. *IEEE Transactions on Power Electronics*, 29(8):3852–3863, August 2014.

[7] H.R. Karshenas, H. Daneshpajooh, A Safaee, A Bakhshai, and P. Jain. Basic families of medium-power soft-switched isolated bidirectional DC-DC converters. In *Power Electronics, Drive Systems and Technologies Conference (PEDSTC), 2011 2nd*, pages 92–97, February 2011.

[8] T. Luth, M.M.C. Merlin, T.C. Green, F. Hassan, and C.D. Barker. High-Frequency Operation of a DC/AC/DC System for HVDC Applications. *IEEE Transactions on Power Electronics*, 29(8):4107–4115, August 2014.

[9] T. Mishima and M. Nakaoka. A Load-Power Adaptive Dual Pulse Modulated Current Phasor-Controlled ZVS High-Frequency Resonant Inverter for Induction Heating Applications. *IEEE Transactions on Power Electronics*, 29(8):3864–3880, August 2014.

[10] N. Mohan, T. Undeland, and W. Robbins. *Power electronics: Converters, applications and design*. John Wiley, Hoboken, NJ, 2003.

[11] M.I Rahman, D. Jovcic, and K.H. Ahmed. Reactive current optmisation for high power dual active bridge DC/DC converter. In *PowerTech (POWERTECH), 2013 IEEE Grenoble*, pages 1–6, June 2013.

[12] J.R. Rodriguez, V. Venegas R, E.L. Moreno-Goytia, F.H. Villa Vargas, and E.D. Castaneda S. Single loop, zero reactive power in dual-active-bridge converters. In *2013 IEEE International Autumn Meeting on Power, Electronics and Computing (ROPEC)*, pages 1–7, November 2013.

[13] D. Segaran. *Dynamic Modelling and Control of Dual Active Bridge Bi-directional DC-DC Converters for Smart Grid Applications*. PhD thesis, Melbourne, February 2006.

[14] D. Segaran, D.G. Holmes, and B.P. McGrath. Comparative analysis of single and three-phase dual active bridge bidirectional DC-DC converters. In *Power Engineering Conference, 2008. AUPEC '08. Australasian Universities*, pages 1–6, December 2008.

[15] D. Segaran, B.P. McGrath, and D.G. Holmes. Adaptive dynamic control of a bi-directional DC-DC converter. In *2010 IEEE Energy Conversion Congress and Exposition (ECCE)*, pages 1442–1449, September 2010.

[16] X. She, X. Yu, F. Wang, and A.Q. Huang. Design and Demonstration of a 3.6-kV - 120-V/10-kVA Solid-State Transformer for Smart Grid Application. *IEEE Transactions on Power Electronics*, 29(8):3982–3996, August 2014.

[17] Xu She, R. Burgos, Gangyao Wang, Fei Wang, and AQ. Huang. Review of solid state transformer in the distribution system: From components to field application. In *2012 IEEE Energy Conversion Congress and Exposition (ECCE)*, pages 4077–4084, September 2012.

[18] Haimin Tao, J.L. Duarte, and M.AM. Hendrix. Three-Port Triple-Half-Bridge Bidirectional Converter With Zero-Voltage Switching. *IEEE Transactions on Power Electronics*, 23(2):782–792, March 2008.

[19] N.D. Weise, G. Castelino, K. Basu, and N. Mohan. A Single-Stage Dual-Active-Bridge-Based Soft Switched AC-DC Converter With Open-Loop Power Factor Correction and Other Advanced Features. *IEEE Transactions on Power Electronics*, 29(8):4007–4016, August 2014.

[20] Zhongming Ye, P.K. Jain, and P.C. Sen. Circulating Current Minimization in High-Frequency AC Power Distribution Architecture With Multiple Inverter Modules Operated in Parallel. *IEEE Transactions on Industrial Electronics*, 54(5):2673–2687, October 2007.

[21] B. Zhao, Q. Song, W. Liu, and Y. Sun. Overview of Dual-Active-Bridge Isolated Bidirectional DC-DC Converter for High-Frequency-Link Power-Conversion System. *IEEE Transactions on Power Electronics*, 29(8):4091–4106, August 2014.